

ARTICLES

Low-Dimensional Manifolds in Reaction–Diffusion Equations. 1. Fundamental Aspects[†]

Michael J. Davis*

Chemistry Division, Argonne National Laboratory, Argonne, Illinois 60439

Received: September 30, 2005; In Final Form: December 19, 2005

The approach to equilibrium for systems of reaction–diffusion equations on bounded domains is studied geometrically. It is shown that equilibrium is approached via low-dimensional manifolds in the infinite-dimensional function space for these dissipative, parabolic systems. The fundamental aspects of this process are mapped out in some detail for single species cases and for two-species cases where there is an exact solution. It is shown how the manifolds reduce the dimensionality of the system from infinite dimensions to only a few dimensions.

I. Introduction

The accurate modeling of reactive flows requires the description of the interplay of chemistry and transport.¹ Generally, the range of time scales for the chemical-kinetic processes describing the chemistry is much larger than that for transport processes, making the inclusion of complex chemical kinetics a challenge. However, it is common for much of the chemistry to relax on time scales shorter than the transport time scales, and it is generally expected that some sort of reduced chemical description can be made so that the modeling of the full process becomes more tractable. A great deal of work has focused on this sort of reduction, and it is reviewed in several places,² where there are also reviews of other types of reduction techniques. Reduction techniques that rely on reduced chemical descriptions can often be viewed as generalizations of the well-known steady-state approximation.³ In addition, there is a large amount of literature on the reduction via perturbation techniques in engineering and applied mathematics that are relevant to the reduction of chemical kinetics and modeling.^{4,5}

One of the modern approaches to kinetic reduction that builds on the steady-state approximation recognizes the geometric^{3,6} character of the approximation. The steady-state approximation is replaced by more accurate representations relying on a better description of the dynamics of the chemical kinetics. Important work by Fraser and Roussel,^{6–9} Lam and Goussis,¹⁰ and Maas and Pope^{11,12} provides the foundations for this approach as well as important insights and techniques. These references have provided the impetus for a number of studies that have followed.^{5,13–21} The methods presented in these references rely on the fact that the approach to equilibrium occurs along lower-dimensional surfaces in the phase space of the species,¹⁵ so-called low-dimensional manifolds.

The methods of reduction that rely on low-dimensional manifolds use techniques borrowed from the dynamical-systems literature.²² Reference 15 has detailed analyses of these ap-

proaches from a dynamical-systems perspective. This paper is the first in a series that extends the dynamical-systems approach to the study of nonlinear partial differential equations involving the interplay between reaction and transport, with the goal of investigating their reduction within a geometric framework. The purpose of these papers is to understand the interplay between transport and chemistry and to try to understand the types of reductions that are possible, particularly when there is no longer a clear separation between kinetics and transport or at time scales so long that slow diffusion is important.

There are several earlier papers that have studied the interplay of reaction and transport within a geometric framework.^{12,18,23,24} Like these references, the current paper focuses on the interplay between kinetics and diffusion, concentrating on systems of dissipative reaction–diffusion equations that relax to a single equilibrium distribution for the chemical species. From earlier work,¹² it is expected that diffusion is more important than advection in making reduced chemical descriptions invalid. Several different small systems are studied here to provide a foundation for what is presented in the paper that follows this one.²⁵ This paper and the follow-up paper concentrate on the final stages of relaxation to equilibrium, while later ones focus on shorter times.²⁶

To make the discussion in this Introduction more concrete, a result is presented for the system studied in ref 25, the combustion of ozone under isothermal conditions and under the influence of diffusion. There are three species that participate: O, O₂, and O₃. The top two panels in Figure 1 show results for O₂. Figure 1a shows the concentration profile of O₂ at two times. The thinner dotted line is at $t = 0$, and the thicker dotted line is at $t = 1$ ms. Figure 1b shows results for a different initial distribution at the same two times, with the thin dashed line showing $t = 0$ and the thicker dashed line $t = 1$ ms. The parameters describing the system are listed in the figure caption. The plots in Figure 1b highlight two pairs of points. Points at $x = 0.49$ are plotted as an open square on the $t = 0$ curve and a filled square on the $t = 1$ ms curve. Points at $x = 0.77$ are plotted as an open diamond on the $t = 0$ curve and a filled diamond on the $t = 1$ ms curve.

[†] Part of the special issue “John C. Light Festschrift”.

* Author to whom correspondence should be addressed. E-mail: davis@tcg.anl.gov.

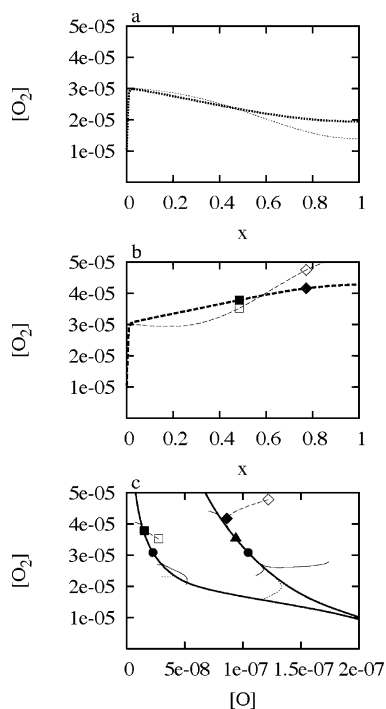


Figure 1. Series of plots for an ozone reaction–diffusion system. Temperature is fixed at 1000 K, with the same kinetic parameters as in refs 18 and 25, and all diffusion constants are fixed at 100.0.²⁵ Figures 1a and 1b show distribution functions for O_2 at two different times propagated from two different initial distributions. In Figure 1c the concentrations of O_2 and O are plotted in phase space. For the set of curves on the left O and O_2 are plotted at $x = 0.49$, and for the right set O is plotted at 0.29 and O_2 at 0.77. The spatial extent of the problem in these scaled units is 0.0 to 1.0. See text for further details.

In Figure 1c results from ozone combustion are plotted in a different manner. There are two sets of curves plotted in Figure 1c. The set of curves on the left of Figure 1c follow the evolution of the distributions from the top two panels by plotting the concentration of O_2 versus the concentration of O at the spatial point $x = 0.49$ for both species (the range is from 0.0 to 1.0). The results for these distributions are plotted with the same line types as they are in Figures 1a and 1b. The symbols on the dashed curve match the symbols on the distributions plotted in Figure 1b. The solid dot shows the equilibrium value of the O_2 and O distributions at $x = 0.49$.

In addition to results for the distributions in the top two panels, there are four other curves on the left side of Figure 1c. Three of these are plotted with thin solid lines and a fourth with a thicker solid line. The three thin-line curves result from the time development of three additional initial distributions. It can be observed in the left part of Figure 1c that all five sets of initial distributions asymptotically approach the thicker solid line. This latter curve is what is referred to as a “low-dimensional manifold”. When a system reaches such a manifold, there is a reduction in the number of partial differential equations that need to be followed. The curve on the left of Figure 1c demonstrates that after ~ 1 ms the concentration of O_2 is a function of O . Plots of O_3 versus O also show a functional relationship. On the low-dimensional manifold the system of partial differential equations has been reduced from three to one, with the behavior of the other two species (O_2 and O_3) described by the functional relationships defined by the low-dimensional manifold.

The curves on the left in Figure 1c demonstrate that all initial distributions relax to equilibrium in a similar manner, first approaching a one-dimensional curve in the space of species

on the way to equilibrium. This is a standard result in the study of low-dimensional manifolds for systems of ordinary differential equations approaching equilibrium. The presence of spatial coordinates and the effects of diffusion may cause modifications to the simplest picture of this process, as refs 18, 23, and 24 indicate, but does not represent a reduction of the system to finite dimensions, because even a single partial differential equation defines an infinite-dimensional dynamical system.

What this paper is focused on is the reduction indicated by the right-hand set of curves in Figure 1c. These curves were generated by plotting the value of the concentration of O_2 versus the concentration of O at *different* spatial points, $x = 0.29$ for O and $x = 0.77$ for O_2 . The figure indicates that this representation also approaches a single curve (thick line), although different than the one on the left of the panel. The dashed and dotted curves on the right correspond to the same pair of initial distributions as on the left set of Figure 1c and the distributions in Figures 1a and 1b. The solid and open diamonds are the points plotted in Figure 1b with the same symbols. The solid dot is the coordinate pair formed from the equilibrium value of O at $x = 0.29$ and O_2 at $x = 0.77$. The solid triangle on the right set of curves is the coordinate pair at $t = 4.6$ ms.

The set of curves on the right in Figure 1c indicates that the system of three partial differential equations is reduced beyond what is implied by the left set of curves. At a time between 1.0 and 4.6 ms the system of partial differential equations has been reduced to a one-dimensional system. At that point it can be described by a single ordinary differential equation and a set of functional relationships between the value of O at a single point and the values of all species (O , O_2 , and O_3) at all other spatial points. The time is set between 1.0 and 4.6 ms based on the fact that the closed diamond on the right and the closed square on the left are both plotted at the same time. The closed square lies on the manifold that describes the reduction of the number of partial differential equations, and the closed diamond on the right does not lie on the manifold describing the reduction to one ordinary differential equation. The solid triangle on the right does indicate that such a final reduction occurs by 4.6 ms.

The purpose of this paper and the follow-up paper²⁵ is to study the process pictured in Figure 1c in detail. The present paper will describe several fundamental aspects of this process, relying mostly on systems for which there is an analytical solution. Reference 25 will use the systems studied in this paper to develop methods to extend the analysis here to systems such as the ozone example in Figure 1.

The outline of this paper is as follows. Section II introduces the notion of an infinite-dimensional phase space for a single diffusion equation. It then shows that the reduction to finite dimensions is a straightforward consequence of dissipation. It then demonstrates how this notion can be extended analytically to an isolated, irreversible unimolecular reaction in the presence of diffusion and numerically to a nonlinear problem, an irreversible association reaction. For this latter case, it is natural to study local, linearized dynamics that is introduced for that single reaction–diffusion equation and extended to systems of nonlinear reaction–diffusion equations in Appendix B.

Sections III and IV extend the analysis of section II to two systems of reaction–diffusion equations that have analytic solutions, one of which is nonlinear (section IV). These sections show the conditions under which attractive one-dimensional and two-dimensional manifolds are relevant for relaxation to equilibrium. The systems studied in these sections are meant to

provide test cases for the methods proposed in ref 25. Section V presents additional discussions and a conclusion. There are seven appendices that provide additional technical details.

II. The Diffusion Equation, Reaction–Diffusion Equations, and Dynamical-Systems Analysis

A. The Diffusion Equation, Infinite-Dimensional Phase Space, and Low-Dimensional Manifolds. An integral part of the description of reactive flows¹ is the notion of diffusion, which is described in one spatial dimension (within a hydrodynamic formulation) as²⁷

$$\frac{\partial y}{\partial t} = D \frac{\partial^2 y}{\partial x^2} \quad (2.1)$$

which assumes a constant diffusivity, D , typically referred to as the diffusion constant. In the context of reactive flows, eq 2.1 is posed as an initial boundary problem.²⁷ The boundary conditions used here are

$$y(x=0) = y_0 \quad \frac{\partial y}{\partial x}(x=1) = 0 \quad (2.2)$$

that are analogous to typical boundary conditions studied in one-dimensional flame calculations,²⁸ where the transport is more complicated because it includes advection and typically has nonconstant diffusivity. Initial conditions are specified as

$$y(x,0) = y_0 + \sum_{n=0}^{\infty} a_n \sin\left(n + \frac{1}{2}\right)\pi x \quad (2.3)$$

where y_0 is the equilibrium distribution of y , which solves

$$0 = D \frac{\partial^2 y}{\partial x^2} \quad (2.4)$$

and has the correct boundary conditions. It is a constant in this case. The sine functions in eq 2.3 are eigenvectors of the Laplacian on the right-hand side of eq 2.1.

As indicated in eq 2.2, for convenience the spatial domain is always chosen to be the unit interval in this paper. Changing D in eq 2.1 is equivalent to changing the spatial domain. For example, changing the length of the spatial domain by a factor r is equivalent to changing the diffusion constant by $1/r^2$.

The solution of eq 2.1 with boundary conditions in eq 2.2, initial conditions in eq 2.3, and an equilibrium distribution satisfying eq 2.4 is

$$y(x,t) = y_0 + \sum_{n=0}^{\infty} a_n e^{-(n+1/2)^2\pi^2Dt} \sin\left(n + \frac{1}{2}\right)\pi x \quad (2.5)$$

Because it takes an infinite number of terms to describe the time development of a distribution, partial differential equations are sometimes referred to as infinite-dimensional dynamical systems.^{29,30}

Homogeneous chemical kinetics is described by ordinary differential equations, and a number of studies of low-dimensional manifolds in chemical kinetics have studied them in the context of the phase space of the chemical species.^{6–9,11,15,18} In analogy to that work, the present paper studies reaction–diffusion equations in a phase space, as indicated already in Figure 1, and this distinguishes the present paper from earlier work on manifolds for partial differential equations describing reaction and diffusion.^{18,23,24} To study the phase space of the

diffusion equation, a specification of spatial location is necessary and the designation

$$y(x_\beta, t) = y_0 + \sum_{n=0}^{\infty} a_n e^{-(n+1/2)^2\pi^2Dt} \sin\left(n + \frac{1}{2}\right)\pi x_\beta \quad (2.6)$$

refers to the evaluation of the distribution $y(x,t)$ at the spatial point x_β . Here and in the rest of the paper displacement of y from equilibrium at x_β ($y(x_\beta, t) - y_0$) will be referred to as y_β , or more generally $y_{k\beta}$, denoting the k th coordinate of an n -dimensional system. A two-dimensional projection of the infinite-dimensional phase space will be designated as a “ y_β/y_σ ” projection. Such projections will be used to study the functional relationship between y_β and y_σ during the time development of the distribution $y(x,t)$, as indicated in Figure 1.

Although the phase space is infinite-dimensional, the diffusion equation is dissipative, as indicated in eq 2.5. As time increases, fewer terms are needed to describe the time development of y because the higher terms become very small and the system effectively becomes a finite-dimensional one. It eventually relaxes to an equilibrium distribution $y = y_0$, which is described by an infinite set of equal coordinates $y_\beta = y_0$ and is a single point in the infinite-dimensional phase space. A single point in the phase space is a zero-dimensional manifold. All of the other cases studied here will have equilibrium distributions that are not spatially constant. These also are single points in the infinite-dimensional phase space but with a set of points $y_\beta = y(x_\beta)$.

Appendix A has a detailed description of the relaxation of the diffusion equation through phase space. A simplified description of this relaxation is presented in this subsection. The final approach to equilibrium for the diffusion equation is described by

$$y(x,t) = y_0 + a_0 \sin \frac{\pi x}{2} e^{-\pi^2Dt/4} \quad (2.7)$$

which is a line in the infinite-dimensional phase space. To define a projection onto the phase space of the species, time and the initial condition are eliminated. First rewrite eq 2.7 and define it at a point x_β

$$a_0 e^{-\pi^2Dt/4} = \frac{y(x_\beta, t) - y_0}{\sin \frac{\pi x_\beta}{2}} \quad (2.8)$$

Then a projection of the line onto the y_β/y_σ plane is defined

$$y_\sigma = \frac{y_\beta}{\sin \frac{\pi x_\beta}{2}} \sin \frac{\pi x_\sigma}{2} \quad (2.9a)$$

$$y_\beta \equiv y(x_\beta) - y_0 \quad y_\sigma \equiv y(x_\sigma) - y_0 \quad (2.9b)$$

The relaxation outlined above is generic for dissipative systems. What makes the notion of a low-dimensional manifold useful is a separation of time scales, characterized here by the attractiveness of a particular manifold. In general, for nonlinear systems, it is difficult to judge such a quantity except in a local linear sense, and often a visual inspection of the phase plane is all that is done. However, in many of the cases studied here, both linear and nonlinear, good global estimates of the attractiveness can be obtained. The basis for this is presented here for the diffusion equation and implemented in several examples in the rest of the paper. Consider the next term in the expansion

of eq 2.7 and evaluate both terms at two different points, written in matrix-vector notation

$$\begin{pmatrix} y_\beta(t) - y_0 \\ y_\sigma(t) - y_0 \end{pmatrix} = \begin{pmatrix} \sin\left(\frac{\pi x_\beta}{2}\right) & \sin\left(\frac{3\pi x_\beta}{2}\right) \\ \sin\left(\frac{\pi x_\sigma}{2}\right) & \sin\left(\frac{3\pi x_\sigma}{2}\right) \end{pmatrix} \begin{pmatrix} a_0 e^{-\pi^2 D t/4} \\ a_1 e^{-9\pi^2 D t/4} \end{pmatrix} \quad (2.10)$$

as well as the initial conditions projected onto the same plane

$$\begin{pmatrix} y_\beta(t=0) - y_0 \\ y_\sigma(t=0) - y_0 \end{pmatrix} = \begin{pmatrix} \sin\left(\frac{\pi x_\beta}{2}\right) & \sin\left(\frac{3\pi x_\beta}{2}\right) \\ \sin\left(\frac{\pi x_\sigma}{2}\right) & \sin\left(\frac{3\pi x_\sigma}{2}\right) \end{pmatrix} \begin{pmatrix} a_0 \\ a_1 \end{pmatrix} \quad (2.11)$$

Inversion of the matrix in eqs 2.10 and 2.11 defines the exponentials

$$e^{-\pi^2 D t/4} = \frac{y_\sigma \sin\left(\frac{3\pi x_\beta}{2}\right) - y_\beta \sin\left(\frac{3\pi x_\sigma}{2}\right)}{y_{\sigma 0} \sin\left(\frac{3\pi x_\beta}{2}\right) - y_{\beta 0} \sin\left(\frac{3\pi x_\sigma}{2}\right)} \equiv \frac{v}{v_0} \quad (2.12a)$$

$$e^{-9\pi^2 D t/4} = \frac{y_\sigma \sin\left(\frac{\pi x_\beta}{2}\right) - y_\beta \sin\left(\frac{\pi x_\sigma}{2}\right)}{y_{\sigma 0} \sin\left(\frac{\pi x_\beta}{2}\right) - y_{\beta 0} \sin\left(\frac{\pi x_\sigma}{2}\right)} \equiv \frac{u}{u_0} \quad (2.12b)$$

with the numerator of eq 2.12b describing the manifold from eq 2.9a. These equations use the definitions from eq 2.9b, with the obvious generalization to define $y_{\beta 0}$ and $y_{\sigma 0}$. Through the use of eqs 2.12a and 2.12b the behavior in phase space is observed to have the following form

$$\frac{u}{u_0} = \left(\frac{v}{v_0}\right)^\alpha \quad (2.13a)$$

$$\alpha = 9 \quad (2.13b)$$

Equation 2.13a states that the system relaxes to the manifold ($u = 0$), and eq 2.13b describes the rate of the attraction. Manifolds whose values of α are too low will not be considered very attractive and not useful for dimension reduction.

The goal of the rest of this paper is to study finite-dimensional manifolds such as those outlined here and in Appendix A for reaction–diffusion equations, both linear and nonlinear, and for systems of reaction–diffusion equations.

B. Reaction–Diffusion Equations. Two examples of one-species cases are used as a further introduction to finite-dimensional manifolds.

1. Irreversible Unimolecular Reaction. The spatio-temporal behavior of a species that diffuses and undergoes an irreversible unimolecular decay is written as

$$\frac{\partial y}{\partial t} = -ky + D \frac{\partial^2 y}{\partial x^2} \quad (2.14)$$

The spatial domain and the boundary conditions are the same as those in section IIA. For the case $k = 0$ the reaction–diffusion equation becomes the diffusion equation discussed in section IIA. The behavior of y is

$$y(x,t) = y^{\text{eq}}(x) + \sum_{n=0}^{\infty} a_n e^{-[k+(n+1/2)^2\pi^2 D]t} \sin\left(n + \frac{1}{2}\right)\pi x \quad (2.15)$$

for the initial distribution

$$y(x,0) = y^{\text{eq}}(x) + \sum_{n=0}^{\infty} a_n \sin\left(n + \frac{1}{2}\right)\pi x \quad (2.16)$$

The equilibrium distribution is

$$y^{\text{eq}}(x) = \frac{y_0}{e^{\sqrt{k/D}} + e^{-\sqrt{k/D}}} [e^{\sqrt{k/D}(x-1)} + e^{-\sqrt{k/D}(x-1)}] \quad (2.17)$$

The results in eqs 2.15–2.17 can be compared to eq 2.5. The two differences between the reactive and nonreactive cases are the nontrivial equilibrium state for the reactive case and a change in the time dependence in the exponential describing the unimolecular decay.

The behavior observed in Figure 1 can be understood for the current reaction–diffusion equation by noting that eq 2.15 indicates an approach to equilibrium whose final stage is one-dimensional and has the form

$$y(x_\beta, t) = y^{\text{eq}}(x_\beta) + a_0 e^{-[k+\pi^2 D/4]t} \sin\left(\frac{\pi x_\beta}{2}\right) \quad (2.18)$$

where the function y is evaluated at the point x_β in the unit interval. Time can be eliminated, and the value of y at a second point, x_σ , can be found as in section IIA and Appendix A

$$y_\sigma = \frac{\sin\left(\frac{\pi x_\sigma}{2}\right)}{\sin\left(\frac{\pi x_\beta}{2}\right)} y_\beta \quad (2.19a)$$

$$y_\beta \equiv y(x_\beta) - y^{\text{eq}}(x_\beta) \quad (2.19b)$$

$$y_\sigma \equiv y(x_\sigma) - y^{\text{eq}}(x_\sigma) \quad (2.19c)$$

which again is a projection of a line from the infinite-dimensional phase space onto a plane. The notation of eq 2.9 has been generalized to include a nonconstant equilibrium distribution. Equation 2.19 demonstrates that the manifold depends on the relative sizes of k and D only through the equilibrium distribution (eq 2.17).

Examples of the projections of the time development of distributions and how they approach the manifold in eq 2.19 are shown in Figure 2 for different initial distributions for $k = y_0 = 1$, $x_\beta = 0.25$, and $x_\sigma = 0.65$. The top panel shows results for $D = 0.1$ and the bottom panel for $D = 10.0$. The solid line shows the projection onto the plane of the linear, one-dimensional manifold. The dashed curves show four “trajectories”, which are the time development of two points along the four different distributions defined in eq 2.16. Comparison of the two panels indicates that as D gets larger the attraction to the manifold gets stronger. In the top panel the dashed lines show that trajectories go almost directly to the equilibrium point, drawn as a solid dot. In the bottom panel the dashed curves are attracted to the manifold much more rapidly, spending a good bit of time on their way to equilibrium.

To understand the approach to the manifold pictured in Figure 2, it is assumed that the initial distribution is generic in the

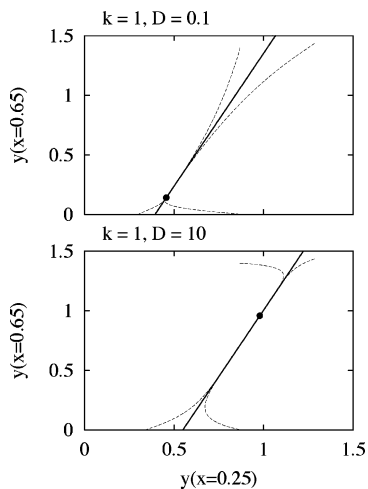


Figure 2. Results for four initial distributions (dashed curves), whose time development is described by eq 2.15. The solid dot shows the value of the equilibrium distribution for these pairs (eq 2.17). Both panels were generated for $k = 1.0$, and the top panel has results for $D = 0.1$, and the bottom for $D = 10.0$. The distributions are monitored at two different points; $x = 0.25$ describes the x -axis, and $x = 0.65$ describes the y -axis. The dashed lines approach a one-dimensional manifold that is described in eq 2.19. When D is smaller than k in the top panel the manifold is less attractive than it is when D is larger than k , as it is in the bottom panel. The relative attractiveness is described by the parameter α , which is defined in eqs 2.21a and 2.21b. For the top panel $\alpha = 2.6$, and for the bottom panel $\alpha = 8.7$ (eq 2.21b).

sense that the summation in eq 2.16 has a reasonable mixture of expansion coefficients, the a_n values, and is not centered mostly on a single component. Then the analysis of section IIA and Appendix A is repeated starting with

$$\begin{pmatrix} y_\beta(t) \\ y_\sigma(t) \end{pmatrix} = \begin{pmatrix} \sin\left(\frac{\pi x_\beta}{2}\right) & \sin\left(\frac{3\pi x_\beta}{2}\right) \\ \sin\left(\frac{\pi x_\sigma}{2}\right) & \sin\left(\frac{3\pi x_\sigma}{2}\right) \end{pmatrix} \begin{pmatrix} a_0 e^{-[k+\pi^2 D/4]t} \\ a_1 e^{-[k+9\pi^2 D/4]t} \end{pmatrix} \quad (2.20)$$

that uses the notation of eq 2.19 and is a slightly modified version of eq 2.10 and ending with the following

$$\frac{u}{u_0} = \left(\frac{v}{v_0}\right)^\alpha \quad (2.21a)$$

$$\alpha = \frac{4k + 9\pi^2 D}{4k + \pi^2 D} \quad (2.21b)$$

To understand these equations more fully, see the derivation of eqs 2.12a and 2.12b. Once again, $u = 0$ defines the manifold of eq 2.19.

Equations 2.21a and 2.21b, as well as Figure 2, demonstrate that the apparent attractiveness of the manifold is controlled by the relative sizes of k and D . Equation 2.21b demonstrates that α can never be greater than 9, the value for the diffusion equation in eq 2.13b. This is different than the case of manifolds for pure chemical-kinetic systems, where the stiffness is controlled by the relative rate constants and can be quite large. Equation 2.21b demonstrates that there is very little attraction unless D is large compared to k , otherwise the relaxation is controlled by the reaction and the manifold is not very attractive at all.

It is also possible to define two-dimensional manifolds, and Appendix G.1 does that for the system studied in this subsection. The rest of the paper will study one-dimensional and two-

dimensional manifolds, because they describe the final approach to equilibrium. It is not hard to define higher-dimensional manifolds for linear systems.

In general, unlike the system studied here, the reactive part of a reaction–diffusion equation is nonlinear, and a less detailed analysis is possible. The next subsection extends some of the analysis to a nonlinear reaction–diffusion equation near equilibrium to demonstrate how some of this analysis is done.

2. Irreversible Association Reaction. The simplest nonlinear reaction–diffusion equation describes an irreversible association reaction

$$\frac{\partial y}{\partial t} = -ky^2 + D \frac{\partial^2 y}{\partial x^2} \quad (2.22)$$

Although this system depends on two parameters, k and D , most of the analysis in this subsection requires only the ratio

$$\eta = \frac{k}{D} \quad (2.23)$$

The equilibrium state satisfies

$$0 = -\eta y^2 + \frac{\partial^2 y}{\partial x^2} \quad (2.24)$$

Through the use of η , eq 2.22 can be rewritten as

$$\frac{\partial y}{\partial \tau_D} = -\eta y^2 + \frac{\partial^2 y}{\partial x^2} \quad (2.25a)$$

with

$$\tau_D = Dt \quad (2.25b)$$

which reveals that the geometric structure of phase space does not change with the transformation, although time is scaled. The importance of η is also clear in the previous subsection, where a similar analysis could be done on eqs 2.15–2.17.

Equation 2.22 is nonlinear in y and analytical solutions such as those in the previous subsection are formidable, even if possible, so a numerical approach is undertaken to solve the equation. The partial differential equation is replaced by a set of ordinary differential equations³¹

$$\frac{dy_k}{dt} = -k(y_k)^2 + \frac{D}{\Delta x^2}(y_{k+1} - 2y_k + y_{k-1}) \quad (2.26)$$

where $y(x,t)$ is defined on a grid of equally spaced spatial points and the second derivative in eq 2.22 is calculated by finite differences. This method is commonly called semidiscrete or method-of-lines. There are much more sophisticated versions of the algorithm.^{31,32} Only points interior to the boundary are propagated with this system of ordinary differential equations. The point on the boundary at $x = 0$ is fixed by the boundary condition as y_0 . In turn, y_0 is used to define y_1

$$\frac{dy_1}{dt} = -k(y_1)^2 + \frac{D}{\Delta x^2}(y_2 - 2y_1 + y_0) \quad (2.27)$$

The point on the right boundary is defined by the no-flux condition in eq 2.2, and the propagation of the rightmost grid point uses this constraint and the formula for backward second differences.³³

Although it is not possible to analytically derive low-dimensional manifolds for eq 2.22, the plots in Figure 3

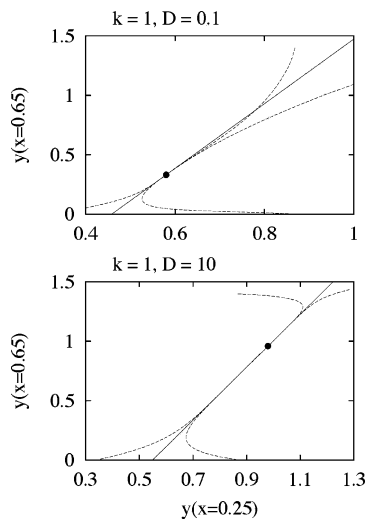


Figure 3. Plots similar to those for Figure 2, but generated for eq 2.22. The top panel demonstrates that the nonlinearity of the system leads to deviation from the linear manifold shown as solid lines in the two panels. The nonlinear system in the top panel is also more attractive than the linear version in Figure 2, with results presented below describing this. The text has further important details.

demonstrate that the system is attracted to a one-dimensional manifold, because of the behavior of the dynamics of the four initial distributions plotted as dashed lines in both panels of Figure 3. The trajectories derived from these distributions appear to be attracted to a one-dimensional curve in both panels of Figure 3, demonstrating that these systems possess one-dimensional manifolds similar to those in Figure 2. The first approximation to a manifold for a nonlinear system is a linear one, and Figure 3 demonstrates that a linear manifold (solid line) almost perfectly describes the strongly attractive case in the bottom panel and is close to the correct manifold in the top panel, based on the behavior of the trajectories. Although the nonlinearity of the system is not manifest to any degree in Figure 3, it has important consequences for the degree of attractiveness of the manifolds. These consequences are most readily analyzed in the vicinity of the equilibrium distribution.

The linear approximations to manifolds pictured in Figure 3 were generated from stability analysis near the equilibrium configuration, which is a generalization to partial differential equations of the stability of equilibrium points in ordinary differential equations.^{34–36} A small displacement in function space away from equilibrium gives the following linear partial differential equation

$$\frac{\partial(\delta y)}{\partial t} = -2ky^{\text{eq}}\delta y + D \frac{\partial^2 \delta y}{\partial x^2} \quad (2.28)$$

where δy describes an infinitesimal displacement in function space away from the equilibrium state $y^{\text{eq}}(x)$. Only when y^{eq} is constant may eq 2.28 generally be solved analytically, usually as a sum over basis states. However, a numerical solution of eq 2.28 can be generated starting with a basis set consisting of the eigenvectors of the diffusion equation, as described in section IIA, or on a grid as is done in eq 2.27. For consistency, this latter technique is used, and a set of ordinary differential equations describing the functional displacements is written

$$\frac{\partial(\delta y_k)}{\partial t} = -2ky_k^{\text{eq}}\delta y_k + \frac{D}{\Delta x^2}(\delta y_{k+1} - 2\delta y_k + \delta y_{k-1}) \quad (2.29)$$

As in eq 2.27, points adjacent to the boundary have a different definition.

Equation 2.29 can be written as a matrix-vector product

$$\frac{\partial}{\partial t} \delta \mathbf{y} = \mathbf{J} \delta \mathbf{y} \quad (2.30)$$

If the eigenvalues of \mathbf{J} are labeled as λ_i and ordered with the lowest in magnitude designated as λ_0 (they are all negative), then the spatio-temporal behavior of the δy_k values is

$$\delta y_k(x,t) = \sum_m a_{km} \Phi_m(x) e^{\lambda_m t} \quad (2.31)$$

Because \mathbf{J} is a real general matrix, it has left eigenvectors described here by the matrix \mathbf{L} and right eigenvectors described by matrix \mathbf{R} ,³⁷ so that diagonalization is written as

$$\lambda = \mathbf{L}^T \mathbf{J} \mathbf{R} \quad (2.32)$$

where “ \mathbf{T} ” refers to the transpose, and the expansion coefficients and eigenvectors in eq 2.32 are

$$\Phi_m(x_k) = R_{mk} \quad (2.33a)$$

$$a_{km} = \sum_i L_{mi}^T \delta y_{i0}(x_k) \quad (2.33b)$$

where it is understood that the R and L values are properly normalized and $\delta y_{i0}(x_k)$ refers to an initial functional displacement on a grid of points.

Equation 2.31 indicates that a small displacement will relax and the analysis of the manifold in the previous subsection can be reproduced *near* the equilibrium distribution y^{eq}

$$y_\sigma = \frac{\Phi_0(x_\sigma)}{\Phi_0(x_\beta)} y_\beta \quad (2.34)$$

with the notation of eq 2.19 again used. The linear manifolds in Figure 3 were calculated using eq 2.34. Because the eigenvector $\Phi_0(x)$ is nearly a sine function when η is small (see below) results are similar to the previous subsection. However, in general, manifolds are not linear, and the top panel in Figure 3 shows some deviation from linearity in the behavior of the trajectories.

Near equilibrium it is possible to look at the attractiveness of the manifolds for eq 2.22, as was done globally in eqs 2.21a and 2.21b. Analysis similar to what was done there defines the generalization of eq 2.21b as

$$\alpha = \frac{\lambda_1}{\lambda_0} \quad (2.35)$$

Through the use of eq 2.35, Figure 4 compares numerical results for the nonlinear equation in this subsection with results for the linear, unimolecular case in eq 2.21b. In the top panel, the dashed line shows the approach to 1.0 for the linear case, and the solid line shows that the nonlinear, association reaction always stays attractive even as η gets large, a situation where diffusion is much slower than reaction. Although the manifold is attractive for the large η case near equilibrium, it is less attractive than the small η cases shown in the top panel, where α approaches an asymptote of 9 and where diffusion is much faster than reaction.

Another aspect of the nonlinear system versus the linear one in the previous subsection is that the ratio of adjacent eigenvalues is smallest for the first two, something not necessarily true in eq 2.21b, at least for large η . This is demonstrated in

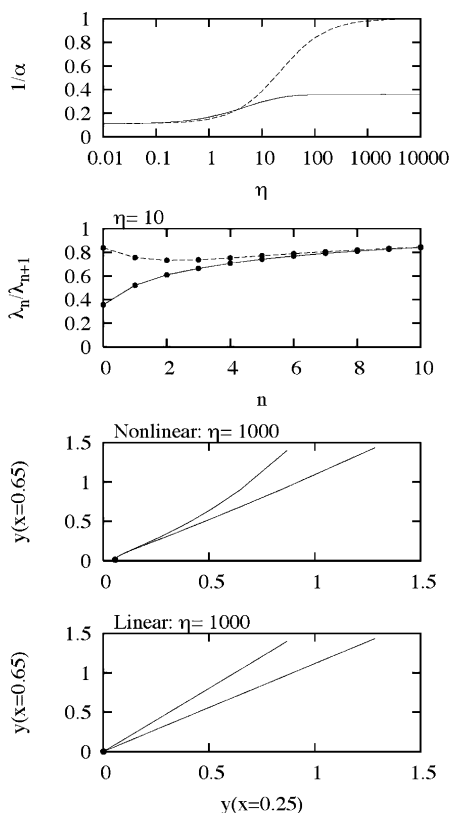


Figure 4. How the attractiveness near equilibrium changes with η (k/D , eq 2.23) for the linear (dashed line) and nonlinear system (solid) described in the text. The linear system approaches 1.0, which is no attraction at all, while the nonlinear system reaches an asymptote of $1/\alpha = 0.36$. The second panel from the top describes the ratio of successive pairs of eigenvalues near equilibrium for the linear (dashed) and nonlinear (solid) systems. This demonstrates that for low-dimensional manifolds, the nonlinear system is more attractive near equilibrium than the linear one for low-dimensional manifolds. The bottom two panels demonstrate how nonlinearity affects the global attractiveness of a manifold, at the same value of η . For the nonlinear system in this subsection (second from bottom) the manifold is much more attractive than it is for the linear case (bottom), as anticipated from the analysis near equilibrium in Figure 1a.

the second panel of Figure 4, where the solid line shows a series of ratios of adjacent eigenvalues for the nonlinear, association reaction and the dashed line shows results for the unimolecular reaction from eq 2.21b, where the ratio reaches a minimum away from $n = 0$. The results in this panel suggest that the one-dimensional manifold for the association reaction is more attractive than higher-dimensional manifolds in the vicinity of the equilibrium distribution and that it is not the most attractive for the linear case, at least when the attractiveness is weak. From our experience with nonlinear reaction–diffusion equations of the type studied in this paper, the degree of attractiveness increases monotonically as the dimension decreases.

The consequences of the attractiveness near equilibrium are evident away from equilibrium, as shown in the third panel of Figure 4. Although the system is not as attractive as the one in the bottom panel of Figure 3, it is much more attractive than the linear case of the previous subsection, which exhibits no attraction at $\eta = 1000$, as shown in the bottom panel.

To further illustrate the effects of nonlinearity, a comparison of the lowest right eigenvectors is shown in Figure 5 at small η (top) and large η (bottom), which are plotted as solid lines. These are compared to $\sin(\pi x/2)$, the lowest eigenvector of the diffusion equation, plotted as a series of dots in the top panel and as a dashed line in the bottom panel. Figure 5 demonstrates

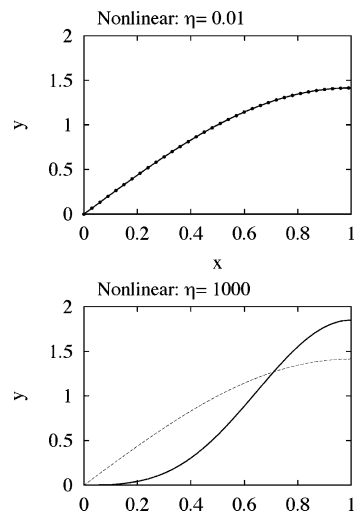


Figure 5. Comparisons to the lowest eigenvectors of \mathbf{J} (eq 2.30) at equilibrium for two values of η . Both panels show the eigenvector as a solid line. In the top panel at low η the eigenvector is almost identical to the eigenvector of the diffusion equation (dots in the top panel). In the bottom panel, at a high η , the eigenvector is very different from the eigenvector of the diffusion equation (dashed line).

that at small η the lowest eigenvector is nearly the same as the linear eigenvector but is far from it at large η . It is clear from Figure 5 that for small η diffusion dominates the attractiveness. For large η , there appears to be a complex interplay between reaction and diffusion and it is difficult to rationalize the form of the eigenvector in the bottom panel of Figure 5 or the asymptotic value of $1/\alpha$ (0.3579) for the solid line in the top panel of Figure 4.

The weak deviation from nonlinearity observed in the top panel of Figure 3 can be more pronounced for systems of nonlinear reaction–diffusion equations, as is clear in Figure 1c, and methods need to be developed to generate them. This will require the extension of some of the analysis in this subsection to systems of nonlinear reaction–diffusion equations, and this is presented in Appendix B.

III. Isomerization with Diffusion

The examples in section IIB demonstrate how the phenomenon in Figure 1 can arise for a single reaction–diffusion equation. The analysis is now extended to systems of reaction–diffusion equations, for a system where the solution once again can be derived in closed form as a summation. Another purpose of this section is to extend the analysis of the competition between reaction and diffusion and the various scenarios where this competition leads to attractive one- and two-dimensional manifolds.

A. The System. Consider the reversible isomerization reaction



Under conditions where the two species diffuse with unequal but constant diffusivities, the spatio-temporal behavior of the system is described by

$$\frac{\partial y_1}{\partial t} = -k_1 y_1 + k_2 y_2 + D_1 \frac{\partial^2 y_1}{\partial x^2} \quad (3.2a)$$

$$\frac{\partial y_2}{\partial t} = k_1 y_1 - k_2 y_2 + D_2 \frac{\partial^2 y_2}{\partial x^2} \quad (3.2b)$$

where the y values refer to concentrations or densities of A and

B and the k values are forward and reverse rate constants. Boundary conditions for both species are the same as those in eq 2.2. The initial distributions

$$y_1(x,0) = y_1^{\text{eq}}(x) + \sum_m b_{1m}(0) \sin\left[\left(m + \frac{1}{2}\right)\pi x\right] \quad (3.3a)$$

and

$$y_2(x,0) = y_2^{\text{eq}}(x) + \sum_m b_{2m}(0) \sin\left[\left(m + \frac{1}{2}\right)\pi x\right] \quad (3.3b)$$

lead to a set of coupled equations for the b values

$$\frac{db_{1m}}{dt} = -\left[k_1 + \left(m + \frac{1}{2}\right)^2 \pi^2 D_1\right] b_{1m} + k_2 b_{2m} \quad (3.4a)$$

$$\frac{db_{2m}}{dt} = k_1 b_{1m} - \left[k_2 + \left(m + \frac{1}{2}\right)^2 \pi^2 D_2\right] b_{2m} \quad (3.4b)$$

The equilibrium distributions satisfy

$$0 = -k_1 y_1^{\text{eq}} + k_2 y_2^{\text{eq}} + D_1 \frac{\partial^2 y_1^{\text{eq}}}{\partial x^2} \quad (3.5a)$$

$$0 = k_1 y_1^{\text{eq}} - k_2 y_2^{\text{eq}} + D_2 \frac{\partial^2 y_2^{\text{eq}}}{\partial x^2} \quad (3.5b)$$

where y_1^{eq} and y_2^{eq} refer to the equilibrium distributions of the two species, with the spatial dependence suppressed. Appendix C describes the full solution of this isomerization example.

B. One-Dimensional Manifolds. The analysis of section IIB is extended to the system of eq 3.1, by using the time development in eqs C.1a and C.1b and the fact that λ_{10} is always the lowest eigenvalue in magnitude. The one-dimensional manifold can be represented in several ways. For example, a spatial value of y_2 can be defined in terms of a spatial value of y_1

$$y_{2\sigma} = \left[\frac{R_{21}^0 \sin\left(\frac{\pi x_\sigma}{2}\right)}{R_{11}^0 \sin\left(\frac{\pi x_\beta}{2}\right)} \right] y_{1\beta} \quad (3.6)$$

and any other spatial value of y_1 can be defined in terms of $y_{1\beta}$ with the following

$$y_{1\sigma} = \frac{\sin\left(\frac{\pi x_\sigma}{2}\right)}{\sin\left(\frac{\pi x_\beta}{2}\right)} y_{1\beta} \quad (3.7)$$

Because the system is linear, the manifolds are straight lines. The notation employed in eqs 3.6 and 3.7 has been adapted from section II. For example

$$y_{1\beta} \equiv y_1(x_\beta) - y_1^{\text{eq}}(x_\beta) \quad (3.8a)$$

$$y_{2\sigma} \equiv y_2(x_\sigma) - y_2^{\text{eq}}(x_\sigma) \quad (3.8b)$$

and the rest of the notation follows. The spatial points x_β and x_σ can be the same or different. Equations 3.6 and 3.7 use $y_{1\beta}$ as the independent variable, but $y_{2\sigma}$ could be used, or some linear

combination. These choices merely fix a projection of the one-dimensional manifold, which is embedded in an infinite-dimensional space. It is straightforward to derive the ratio R_{21}^0/R_{11}^0 , but it is not included in the paper, although it is used in the calculations.

C. Attraction to the One-Dimensional Manifolds. The analysis of the approach to the one-dimensional manifold follows from Appendix D. Because the analysis assumes the final attraction is from a two-dimensional manifold, the approach depends on whether the system parameters define it as a manifold of type 1 or type 2 (Appendix G.2). For type 1, the approach to the one-dimensional manifold on a $y_{2\sigma}/y_{1\beta}$ projection is written in the usual form

$$\frac{u_1}{u_1^0} = \left(\frac{u_2}{u_2^0}\right)^{\alpha_1} \quad (3.9a)$$

$$\alpha_1 = \frac{\lambda_{11}}{\lambda_{10}} \quad (3.9b)$$

The coordinates u_1 and u_2 are

$$\frac{u_1}{u_1^0} = \frac{R_{21}^0 y_{1\beta} \sin\left(\frac{\pi x_\sigma}{2}\right) - R_{11}^0 y_{2\sigma} \sin\left(\frac{\pi x_\beta}{2}\right)}{R_{21}^0 y_{1\beta}^0 \sin\left(\frac{\pi x_\sigma}{2}\right) - R_{11}^0 y_{2\sigma}^0 \sin\left(\frac{\pi x_\beta}{2}\right)} \quad (3.10a)$$

$$\frac{u_2}{u_2^0} = \frac{R_{21}^1 y_{1\beta} \sin\left(\frac{3\pi x_\sigma}{2}\right) - R_{11}^1 y_{2\sigma} \sin\left(\frac{3\pi x_\beta}{2}\right)}{R_{21}^1 y_{1\beta}^0 \sin\left(\frac{3\pi x_\sigma}{2}\right) - R_{11}^1 y_{2\sigma}^0 \sin\left(\frac{3\pi x_\beta}{2}\right)} \quad (3.10b)$$

where $y_{1\beta}^0$ and $y_{2\sigma}^0$ are the obvious generalizations of eqs 3.8.

For type 2 manifolds (eq G.2b), the approach is

$$\frac{u_1}{u_1^0} = \left(\frac{u_2}{u_2^0}\right)^{\alpha_2} \quad (3.11a)$$

$$\alpha_2 = \frac{\lambda_{20}}{\lambda_{10}} \quad (3.11b)$$

with the following coordinates

$$\frac{u_1}{u_1^0} = \frac{-R_{21}^0 y_{1\beta} \sin\left(\frac{\pi x_\sigma}{2}\right) + R_{11}^0 y_{2\sigma} \sin\left(\frac{\pi x_\beta}{2}\right)}{-R_{21}^0 y_{1\beta}^0 \sin\left(\frac{\pi x_\sigma}{2}\right) + R_{11}^0 y_{2\sigma}^0 \sin\left(\frac{\pi x_\beta}{2}\right)} \quad (3.12a)$$

$$\frac{u_2}{u_2^0} = \frac{R_{22}^0 y_{1\beta} \sin\left(\frac{\pi x_\sigma}{2}\right) - R_{12}^0 y_{2\sigma} \sin\left(\frac{\pi x_\beta}{2}\right)}{R_{22}^0 y_{1\beta}^0 \sin\left(\frac{\pi x_\sigma}{2}\right) - R_{12}^0 y_{2\sigma}^0 \sin\left(\frac{\pi x_\beta}{2}\right)} \quad (3.12b)$$

D. Numerical Examples. As outlined above and in Appendix G.2, the attractiveness of the one- and two-dimensional manifolds and the nature of the two-dimensional manifolds depend on the ordering of the eigenvalues, which in turn depends on the relationship of the rate and diffusion parameters k_1 , k_2 , D_1 , and D_2 , as indicated in eqs 3.11a and 3.11b and the eigenvalues presented in Appendix C. All possible scenarios for the nature of the one- and two-dimensional manifolds can be summarized with three parameters

$$\zeta_1 = \frac{D_1 + D_2}{k_1 + k_2} \quad (3.13a)$$

$$\zeta_2 = \frac{D_1 - D_2}{k_1 + k_2} \quad -\zeta_1 \leq \zeta_2 \leq \zeta_1 \quad (3.13b)$$

$$\zeta_3 = \frac{k_1 - k_2}{k_1 + k_2} \quad -1 \leq \zeta_3 \leq 1 \quad (3.13c)$$

The parameter ζ_1 fixes the relative size of the diffusion versus reaction, and the other two parameters fix the actual values of the attractiveness defined in section IIIA. The attractiveness of the one-dimensional manifolds for the two types of manifolds (eqs G.2a and G.2b) are

$$\alpha_1 = \frac{\lambda_{11}}{\lambda_{10}} = \frac{4 + 9\pi^2\zeta_1 - \sqrt{16 + 72\pi^2\zeta_2\zeta_3 + 81\pi^4\zeta_2^2}}{4 + \pi^2\zeta_1 - \sqrt{16 + 8\pi^2\zeta_2\zeta_3 + \pi^4\zeta_2^2}} \quad (3.14a)$$

or

$$\alpha_2 = \frac{\lambda_{20}}{\lambda_{10}} = \frac{4 + \pi^2\zeta_1 + \sqrt{16 + 8\pi^2\zeta_2\zeta_3 + \pi^4\zeta_2^2}}{4 + \pi^2\zeta_1 - \sqrt{16 + 8\pi^2\zeta_2\zeta_3 + \pi^4\zeta_2^2}} \quad (3.14b)$$

Figure 6 summarizes the attractiveness of the one-dimensional manifolds at three values of ζ_1 : 0.1, 1.0, and 10. In physical terms, these refer to situations where reaction is fast compared to diffusion, where diffusion and reaction compete, and where diffusion is fast compared to reaction. These plots show contours of constant α , calculated from the ratio of the first two eigenvalues. The dashed lines in the panels show the boundaries between the different cases. In the panels, contours are drawn from $\alpha = 2.0$ to $\alpha = 8.0$ in increments of 1.0. The lowest contour is drawn as a dotted line, the largest contour at 8.0 as a thick solid line, and the other contours with normal solid lines. In the top panel the minimum contour value is 4.0, and in the bottom two it is 2.0. In all the panels, the largest region is labeled. The largest region in the top panel is case 1, and the largest regions in the bottom two panels are case 2.

Figure 6 demonstrates that the attractiveness of manifolds is dependent on the relative rate of diffusion versus reaction, as measured by ζ_1 . When diffusion is slow compared to reaction as it is in the top panel of Figure 6, there is a very wide range of systems with highly attractive one-dimensional manifolds. When ζ_1 is larger in the bottom two panels of Figure 6 there is a much narrower range of systems where there are highly attractive manifolds. The top panel of Figure 6 also indicates that systems with the most attractive manifolds lie along a ridge where

$$\frac{D_1 - D_2}{D_1 + D_2} \cong \frac{k_1 - k_2}{k_1 + k_2} \quad (3.15)$$

that indicates that the relative difference in the diffusion rates is similar to the relative reaction rates.

As diffusion and reaction become comparable in the middle panel of Figure 6 and then diffusion becomes greater than reaction in the bottom panel, the range of systems that exhibit strongly attractive manifolds first narrows (middle panel) but then begins to become larger in the bottom panel. Also, the conditions for highly attractive manifolds changes in the bottom

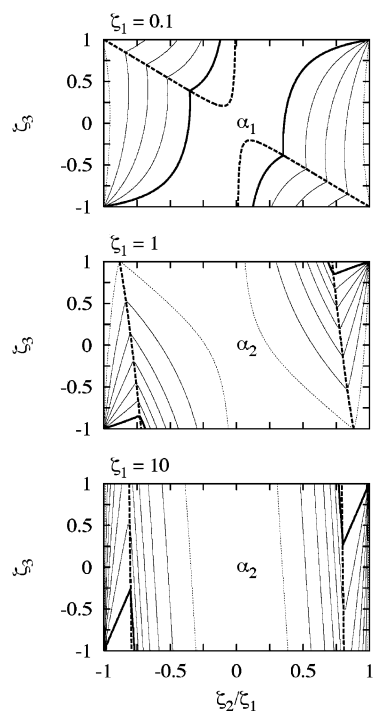


Figure 6. Attractiveness of the one-dimensional manifolds at three values of ζ_1 (eq 3.13a). The contours show values of α ranging from a minimum (dotted lines) to the maximum of 8.0 (solid lines). In the top panel, the minimum contour is at 4.0, and in the bottom two the minimum contour is 2.0. The dashed curves delineate the change from case 1 to case 2 outlined in the text.

two panels compared to eq 3.15, and for these latter examples the attractiveness depends on the faster reacting species also diffusing rapidly: if $D_1 > D_2$, then $k_1 > k_2$, and vice versa.

The two scenarios for attractive one-dimensional manifolds rely on a separation of time scales. The separation of time scales happens in two ways. The first way is observed in the top panel and is separation of time scales between the two physical processes; the diffusion is slow compared to reaction. The other scenario is evident in the bottom panel and involves a separation of time scale between species; one species is slow to react and slow to diffuse, and the other is fast to react and fast to diffuse.

Figure 7 summarizes the attractiveness of the two-dimensional manifolds, for the same three values of ζ_1 as Figure 6. Contour values for the bottom plot follow the conventions of Figure 6, but the top two plots are much flatter and only one contour value (2.0) is plotted on the top panel and four on the middle. The highest point on the top panel is $\alpha = 2.8$. The middle panel contours start with 2.0 and end with 5.0. The lowest contour at 2.0 is plotted with a dotted line and the highest at 5.0 with a thick solid line. Seams are again plotted as dashed lines in Figure 7 and separate three cases, labeled 1–3, which follow the conventions of eq G.7. A comparison of Figures 6 and 7 indicates that systems that have the most attractive one-dimensional manifolds have relatively unattractive two-dimensional manifolds, and vice versa.

Figure 7 demonstrates the physical conditions under which two-dimensional manifolds are most attractive. When diffusion is slow (top panel), two-dimensional manifolds are not very attractive. The situation changes somewhat in the middle panel, which has a maximum value of $\alpha = 5.3$. It demonstrates that the most attractive manifolds are for $D_1 \cong D_2$. In the bottom panel the same condition leads to even more attractive manifolds

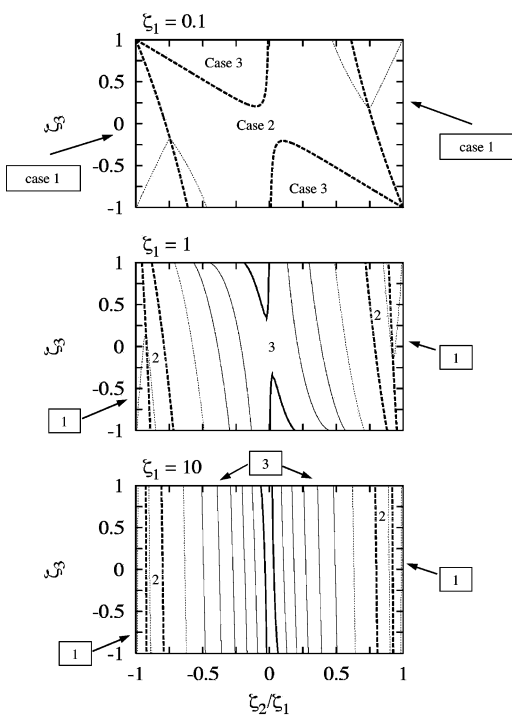


Figure 7. Contour plots presented to depict the attractiveness of the two-dimensional manifolds. The designations on each plot list the cases. These are generated for the same three values of ζ_1 as Figure 6. The maximum contour is plotted with a thick solid line in the bottom two panels, and the minimum value is shown as a dotted line in those panels. In the middle panel the contours range from 2.0 to 5.0, and in the bottom panel from 2.0 to 8.0. The top panel shows a single contour at a value of 2.0 (maximum value is 2.78). The dashed lines depict the seams between the cases. The designations “case 1”, “case 2”, and “case 3” refer to α_{11} , α_{12} , and α_{22} , respectively.

with the maximum α being 8.3. Figure 7 indicates that the maximum attractiveness of two-dimensional manifolds is for systems where both species diffuse faster than they react and do so at approximately an equal rate. These conditions lead to a system that behaves in a manner similar to a pure diffusion equation, such as the one studied in section IIA.

The behavior of systems as they approach the one-dimensional manifolds is shown in Figure 8. These plots show $y_{1\beta}/y_{2\sigma}$ projections of the one-dimensional manifolds (eq 3.6), with manifolds plotted as thick solid lines and equilibrium positions as large solid dots. Results for the propagation of four different initial distributions are plotted as dashed lines in all the panels. Values for x_β and x_σ are listed in the axes labels. Figure 8 demonstrates the qualitative differences in the attractiveness of the manifolds. The behavior of trajectories in Figure 8 can be compared to the values of α . For example, the plot on the upper left shows a system whose one-dimensional manifold is strongly attractive and $\alpha = 8.7$. The system on the upper right has a manifold that is not very attractive, with the system relaxing almost directly to equilibrium. It has a value of α of 1.5.

A two-dimensional manifold is studied in Figure 9 for the system on the upper right of Figure 8. A $y_{1\beta}/y_{2\sigma}/y_{2\phi}$ projection is used. The one-dimensional manifold in Figure 8 has $\alpha = 1.5$, and the two-dimensional manifold in Figure 9 has $\alpha = 5.9$. This relative difference is evident in the comparison of the panel in Figure 8 and the plot in Figure 9. There is almost no attraction to the one-dimensional manifold in Figure 8, but a strong attraction to the two-dimensional manifold in Figure 9. The separation of time scales for the system in Figure 9 is one of the cases discussed for Figure 7. D_1 and D_2 are close enough

that the system is similar to the one-dimensional diffusion equation, with pairs of eigenvalues in the isomerization case being similar to single eigenvalues in the diffusion equation example.

IV. A Nonlinear Reaction–Diffusion System

The analysis of systems of reaction–diffusion equations is now extended to one which is nonlinear but which has a closed form solution in terms of a summation. This system once again will be studied for how the competition between reaction and diffusion affects the low-dimensional manifolds. In addition, because of the nonlinearity it will provide a test for the numerical methods developed in the subsequent paper.²⁵

A. The System and Its Solution. The analysis in section III is extended to a nonlinear system

$$\frac{\partial y_1}{\partial t} = -y_1 + D_1 \frac{\partial^2 y_1}{\partial x^2} \quad (4.1a)$$

$$\frac{\partial y_2}{\partial t} = -\gamma y_2 + a y_1^2 + D_2 \frac{\partial^2 y_2}{\partial x^2} \quad (4.1b)$$

with boundary conditions defined in eq 2.2 and the initial conditions of eq 3.3. All of the results presented here were generated for $a = \gamma - 2$, because the kinetics part of the problem has a simple one-dimensional manifold: $y_2 = y_1^2$ (eq 2.6 in ref 15). The coupled equations for the expansion coefficients are

$$\frac{db_{1m}}{dt} = -\left[1 + \left(m + \frac{1}{2}\right)^2 \pi^2 D_1\right] b_{1m} \quad (4.2b)$$

$$\frac{db_{2m}}{dt} = -\left[\gamma + \left(m + \frac{1}{2}\right)^2 \pi^2 D_2\right] b_{2m} - 2a \sum_j S_j^m b_{1j} + a \sum_k \sum_n r_{kn}^m b_{1k} b_{1n} \quad (4.2b)$$

where the following two integrals have been defined

$$r_{kn}^m = 2 \int \sin\left[\left(m + \frac{1}{2}\right)\pi x\right] \sin\left[\left(k + \frac{1}{2}\right)\pi x\right] \sin\left[\left(n + \frac{1}{2}\right)\pi x\right] dx \quad (4.3a)$$

$$S_j^m = 2 \int y_1^{\text{eq}} \sin\left[\left(m + \frac{1}{2}\right)\pi x\right] \sin\left[\left(j + \frac{1}{2}\right)\pi x\right] dx \quad (4.3b)$$

It is possible to explicitly calculate these integrals, but this is not presented anywhere in the paper. The results presented in the rest of this section include the correct value for them.

Appendix E presents the solution to eqs 4.2a and 4.2b. Equation E.1a has the solution for y_1 , which is derived directly from the diffusion equation. The solution for y_2 is presented in eq E.1b. The solution of y_1 is repeated, along with a concise form for y_2

$$y_1(x,t) = y_1^{\text{eq}}(x) + \sum_{m=0} b_{1m} \sin\left[\left(m + \frac{1}{2}\right)\pi x\right] e^{-[1+(m+1/2)^2\pi^2 D_1]t} \quad (4.4a)$$

$$y_2(x,t) = y_2^{\text{eq}}(x) + \sum_m [c_{1m}(t) + c_{2m}(t) + c_{3m}(t)] \sin\left[\left(m + \frac{1}{2}\right)\pi x\right] \quad (4.4b)$$

The time-dependent coefficients are

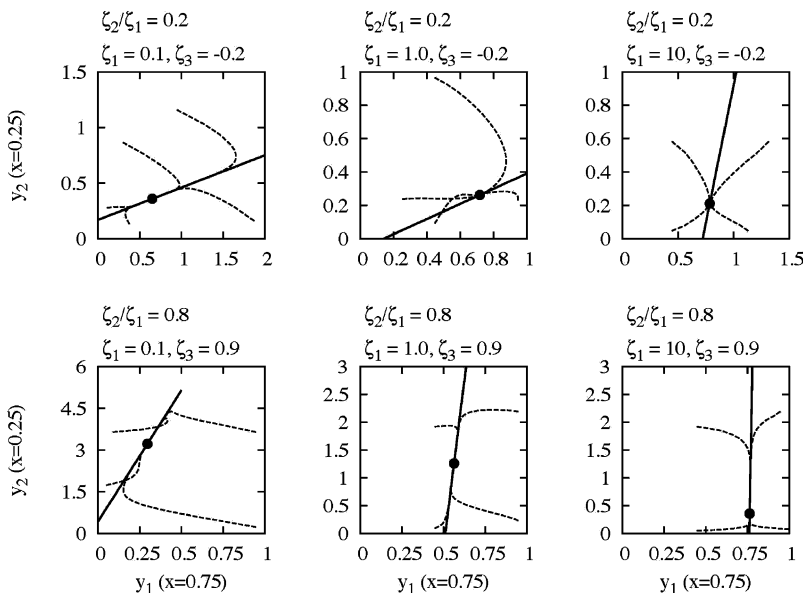


Figure 8. Several examples of the way distributions approach the one-dimensional manifolds. The labeling on the top of each panel lists the values of the ζ_i that are presented in the panel, and these can be compared to the contour plots in Figure 6. In turn, these can be compared to the relative attractiveness evident in the plots. For example, in the panel on the top left, the manifold (solid line) is very attractive, and in the panel on the top right it is not attractive. In this latter case, “trajectories” (dashed curves) go directly to equilibrium (the solid dots in all the panels).

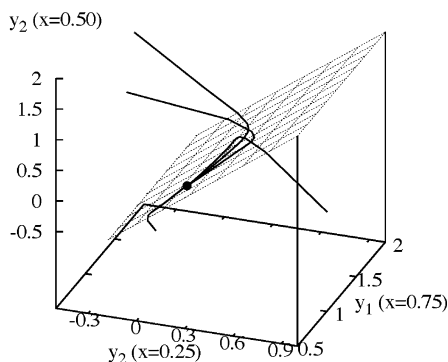


Figure 9. An example of an attractive two-dimensional manifold. This is for the same case as the panel on the top right of Figure 8. Note how there is attraction to the plane (defined in eq G.3) but not to the one-dimensional manifold (eq 3.6).

$$c_{1m}(t) = c_{1m}(0) e^{-[\gamma+(m+1/2)^2\pi^2D_2]t} \quad (4.5a)$$

$$c_{2m}(t) = \sum_k \sum_n d_{kn}^m e^{-\{2+[(k+1/2)^2+(n+1/2)^2]\pi^2D_1\}t} \quad (4.5b)$$

$$c_{3m}(t) = \sum_j e_j^m e^{-[1+(j+1/2)^2\pi^2D_1]t} \quad (4.5c)$$

The coefficients shown in these equations can be derived from eq E.1.

B. One-Dimensional and Two-Dimensional Manifolds. Equations E.2–E.4 present the information necessary for defining and evaluating one-dimensional and two-dimensional manifolds. Although the system is nonlinear and there are no global eigenvalues, equations for the one-dimensional and two-dimensional manifolds can be derived, with the results for the two-dimensional manifolds described in Appendix G.3. They depend on quantities that are obvious from the solution in Appendix E and laid out explicitly in eqs E.4a–E.4c. As in section III, there are several cases, which are ordered here in these pairs

$$\text{case 1}_1 \quad 1 + \frac{\pi^2 D_1}{4} < 1 + \frac{9\pi^2 D_1}{4} \quad (4.6a)$$

$$\text{case 1}_2 \quad 1 + \frac{\pi^2 D_1}{4} < \gamma + \frac{\pi^2 D_2}{4} \quad (4.6b)$$

$$\text{case 2}_1 \quad \gamma + \frac{\pi^2 D_2}{4} < \gamma + \frac{9\pi^2 D_2}{4} \quad (4.6c)$$

$$\text{case 2}_1 \quad \gamma + \frac{\pi^2 D_2}{4} < 1 + \frac{\pi^2 D_1}{4} \quad (4.6d)$$

For case 1, the one-dimensional manifold is most easily represented with $y_{1\beta}$ as an independent variable and points on the y_1 -distribution and y_2 -distribution defined via the manifold as

$$y_{1\sigma} = \frac{\sin\left(\frac{\pi x_\sigma}{2}\right)}{\sin\left(\frac{\pi x_\beta}{2}\right)} y_{1\beta} \quad (4.7a)$$

$$y_{2\phi} = \tau_{20}(x_\phi) \frac{y_{1\beta}^2}{\left(\sin\frac{\pi x_\beta}{2}\right)^2} + \tau_{30}(x_\phi) \frac{y_{1\beta}}{\sin\frac{\pi x_\beta}{2}} \quad (4.7b)$$

Equation 4.7a has been presented in earlier sections (e.g., section II). To derive eq 4.7b, start with the longest time behavior of y_1 and y_2

$$y_{1\beta} = b_{10} \sin\left(\frac{\pi x_\beta}{2}\right) e^{-(1+\pi^2 D_1/4)t} \quad (4.8a)$$

$$y_{2\phi} = b_{10} \tau_{30}(x_\phi) e^{-(1+\pi^2 D_1/4)t} + b_{10}^2 \tau_{20}(x_\phi) e^{-(2+\pi^2 D_1/2)t} \quad (4.8b)$$

The τ values are defined in Appendix E. Equation 4.8a is used to define

$$b_{10} e^{-(1+\pi^2 D_1/4)t} = \frac{y_{1\beta}}{\sin\left(\frac{\pi x_\beta}{2}\right)} \quad (4.9)$$

which is substituted into eq 4.8b to derive eq 4.7b.

It is also straightforward to use y_2 as the independent variable for the one-dimensional manifold for case 1. In this coordinate system, points for the y_1 and y_2 -distributions are

$$y_{1\sigma} = \kappa(x_\beta) \sin\left(\frac{x_\sigma}{2}\right) \quad (4.10a)$$

$$y_{2\phi} = \tau_{20}(x_\phi) \kappa^2(x_\beta) + \tau_{30}(x_\phi) \kappa(x_\beta) \quad (4.10b)$$

$$\kappa(x_\beta) = \frac{-\tau_{30}(x_\beta) \pm \sqrt{[\tau_{30}(x_\beta)]^2 + 4y_{2\beta}\tau_{20}(x_\beta)}}{2\tau_{20}(x_\beta)} \quad (4.10c)$$

For case 2, the manifold follows from the examples in section II and is represented as

$$y_1(x) = y_1^{\text{eq}}(x) \quad (4.11a)$$

$$y_{2\sigma} = \frac{\sin\left(\frac{\pi x_\sigma}{2}\right)}{\sin\left(\frac{\pi x_\beta}{2}\right)} y_{2\beta} \quad (4.11b)$$

C. Attraction to the One-Dimensional Manifold. It is possible to study the approach to the one-dimensional and two-dimensional manifolds presented in the previous subsection. Because of the complexity of the terms to describe attraction to the two-dimensional manifolds, this is left out of the discussion, and only numerical examples are shown in the next subsection.

As in section III, it is assumed that a hierarchy of manifolds exists and that to a good approximation the final approach to the one-dimensional manifold starts on a two-dimensional manifold. There are thus four cases to consider, as outlined above in eq 4.6. The coordinates used follow the form in section III

$$\frac{u_1}{u_1^0} = \left(\frac{u_2}{u_2^0}\right)^{\alpha_{ij}} \quad (4.12)$$

where the subscript “ ij ” refers to the four cases. Appendix F describes the u -coordinates for all the cases.

D. Numerical Examples. To study the manifolds it is useful again to define three variables, as was done in section IVD

$$\xi_1 = \frac{D_1 + D_2}{\gamma + 1} \quad (4.13a)$$

$$\xi_2 = \frac{D_1 - D_2}{\gamma + 1} \quad -\xi_1 \leq \xi_2 \leq \xi_1 \quad (4.13b)$$

$$\xi_3 = \frac{\gamma - 1}{\gamma + 1} \quad -1 \leq \xi_3 \leq 1 \quad (4.13c)$$

For one-dimensional manifolds, the attractiveness can be written with these parameters as

$$\alpha_{11} = \frac{4(1 - \xi_3) + 9\pi^2(\xi_1 + \xi_2)}{4(1 - \xi_3) + \pi^2(\xi_1 + \xi_2)} \quad (4.14a)$$

$$\alpha_{12} = \frac{4(1 + \xi_3) + \pi^2(\xi_1 - \xi_2)}{4(1 - \xi_3) + \pi^2(\xi_1 + \xi_2)} \quad (4.14b)$$

$$\alpha_{21} = \frac{4(1 + \xi_3) + 9\pi^2(\xi_1 - \xi_2)}{4(1 + \xi_3) + \pi^2(\xi_1 - \xi_2)} \quad (4.14c)$$

$$\alpha_{22} = \frac{4(1 - \xi_3) + \pi^2(\xi_1 + \xi_2)}{4(1 + \xi_3) + \pi^2(\xi_1 - \xi_2)} \quad (4.14d)$$

Figure 10 summarizes the values of α for three values of ξ_1 . The convention for contours is the same as in Figures 6 and 7. The lowest contour is at 2.0 and drawn with a dotted line, and the highest contour is at 8.0 and plotted with a thick solid line. The dashed lines in this plot delineate the four cases in eqs 4.6 and 4.14, which are labeled on the plots.

The top panel in Figure 10 demonstrates that the most attractive one-dimensional manifolds for the case where diffusion is relatively small compared to reaction occurs under “stiff” reaction conditions, that is when γ is large or small, because maxima are near ξ_3 values of 1 or -1 . Furthermore, the top panel demonstrates that attractiveness is favored for $D_2 > D_1$ ($\xi_2 < 0$) when γ is large and it is favored for $D_1 > D_2$ when γ is small.

The middle and bottom panels in Figure 10 indicate that once again attractive manifolds are more likely under stiffer reaction conditions, although this restriction is relaxed to a good degree in the bottom panel, where diffusion is fast compared to reaction. In that case the $\alpha = 8.0$ contour value on the left side of the panel describes systems whose value of γ is a minimum of 1.9.

Because they are numerous, the eight cases for the attractiveness of the two-dimensional manifolds are not explicitly written here. Figure 11 summarizes their values for the same three values of ξ_1 as in Figure 11. Once again, when diffusion is small compared to reaction, the two-dimensional manifolds are not very attractive as indicated in the top panel of Figure 11 (see Figure 7). The two-dimensional manifolds become increasingly more attractive as diffusion becomes larger than reaction.

Figure 11 can be compared to the analogous set of plots for isomerization in Figure 7. These two plots give close to the same picture. When diffusion is greater than reaction two-dimensional manifolds are more attractive. There are a few differences between the sets of plots. Some differences are due to the definition of ξ_3 in the two cases. However, there is an additional maximum in the top panel of Figure 11 compared to Figure 7, and the maximum has moved to the middle panel of Figure 11 compared to Figure 7, with a significantly higher maximum (6.7 vs 5.3). The middle panel of Figure 11 demonstrates that the most attractive manifolds are when reaction and diffusion are comparable and both rates of reaction are equal as are the two diffusion constants.

Figure 12 summarizes the one-dimensional manifolds for the systems studied in Figure 10. The top row shows a series of manifolds generated at the same three values of ξ_1 as in Figure 10. They were chosen from systems that follow the $\alpha = 8.0$ contours in Figure 10, which are on the positive ξ_3 halves of the panels, case 1 manifolds (eq 4.7). All of the plots in the top row of Figure 12 are $y_{1\beta}/y_{2\sigma}$ projections. The value of x_β is fixed at 0.25 and x_σ at 0.75. The bottom row in Figure 12 shows a

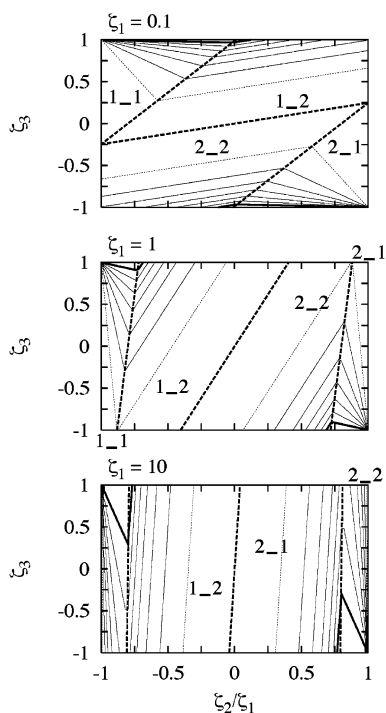


Figure 10. Plots analogous to the ones in Figure 6, with the designations of the cases corresponding to eq 4.6.

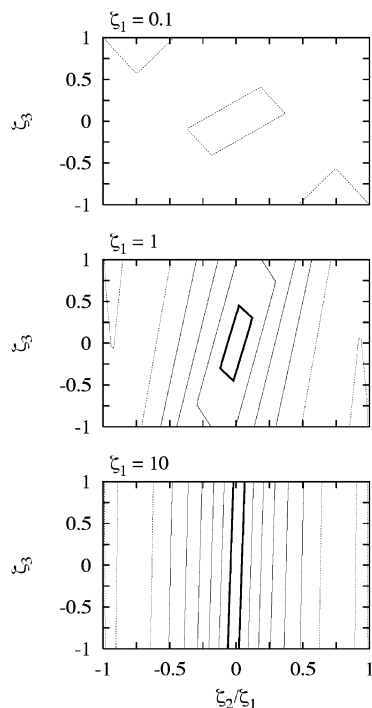


Figure 11. Plots for the nonlinear system in section IV analogous to those in Figure 7 for the isomerization reaction. The algorithm for plotting contours is the same as in Figure 7. No seams are plotted, nor are any designations for manifolds shown, as they were in Figure 7.

different set of projections for $\zeta_1 = 0.1$, the system from the top left corner of Figure 12, and these are evident from the axes labels. They include a $y_{2\beta}/y_{2\sigma}$ projection on the bottom right. As expected from eq 4.7, these manifolds are parabolic, and due to this nonlinearity, they provide good test cases for the methods in ref 25. Although the parabolic form of the manifolds is obvious from eq 4.7, the details of the shape are not transparent, due to the presence of the functions τ_{20} and τ_{30} in eq 4.7a, which are defined in Appendix E. A more complete

analysis of these functions reveals that although the $m = 0$ terms in eqs E.6a and E.7a are by far the largest, there are still significant contributions from $m > 0$.

Further information concerning manifolds is presented in Figure 13. A set of distributions is plotted along one of the manifolds for $\zeta_1 = 0.1$ from Figure 12. The distribution for species 1 is plotted as a solid line and the distribution for species 2 as a dashed line. The small parabola in each panel indicates the location of the distribution along the manifold with a large solid dot. Figure 13 is presented to emphasize that a point along the manifold defines a distribution. It is truly a one-dimensional manifold embedded in an infinite-dimensional function space.

The analysis of the manifolds for the nonlinear reaction–diffusion model is completed in Figure 14. These panels show how distributions relax to one of the manifolds presented in Figure 12. The solid lines in the panels show the manifolds, and the solid dot on each indicates the equilibrium value for that projection. It can be observed that the dashed lines are rather strongly attracted to the one-dimensional manifolds, indicative of the relatively large value of α (8.0) for all of the plots.

V. Conclusion

This paper has explored the approach to equilibrium for reaction–diffusion equations on bounded domains under conditions where there is a single equilibrium state. The study has been restricted to one spatial dimension and one or two species. The purpose of this paper has been to show how such systems approach equilibrium along low-dimensional manifolds in the infinite-dimensional function space. It has been shown that attractive one-dimensional and two-dimensional manifolds exist for these systems over a broad range of system parameters, but the attractiveness is limited compared to that of manifolds for the chemical-kinetic models without diffusion (for example, ref 15), as an investigation of the attractive properties has shown.

This paper sets the stage for the numerical algorithms presented in the next paper.²⁵ For the most part the systems studied here have manifolds that can be represented analytically. The analytical systems will provide important test cases for the methods presented in ref 25 and include a system (section IV) that is nonlinear. In the context of this paper they have provided simple test cases to understand the ways that the manifolds can be represented.

The only system studied here that required a numerical analysis is the one in section IIB.2, and this led to a more complete description of local linear dynamics presented in Appendix B. This analysis will become important in the next paper, where it is employed for generating accurate low-dimensional manifolds. The reaction–diffusion equation in section IIB.2 is also important, because it demonstrated that nonlinearity could lead to manifolds that are more attractive than corresponding ones for linear systems.

No attempt has been made here to connect this work to a large body of literature on “inertial manifolds” for partial differential equations.^{29,30} The definition of “inertial manifold” requires certain conditions, which have not been fully investigated here. It appears that the main condition, exponential attraction,³⁸ is met for most of the systems. However, it is not clear that the system of Figure 1, other systems in ref 25, and the system of section IIB.2 have exponential attraction. These systems have second-order kinetics, which is not exponential. However, any difference between the manifolds studied here and inertial manifolds appears to be one of strict mathematical definition, because they are finite-dimensional manifolds em-

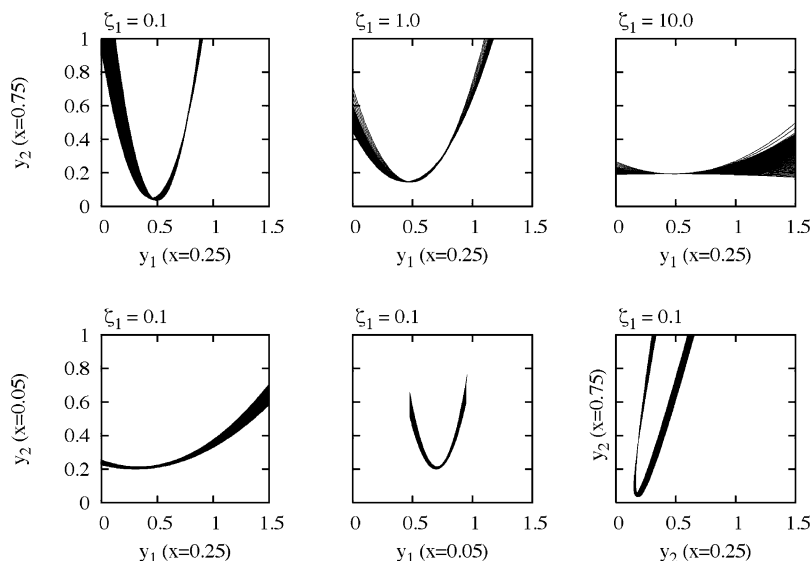


Figure 12. Plots showing how one-dimensional manifolds (eq 4.10) change shape along the contour $\alpha = 8.0$ in Figure 10, for case 1. The projections are defined in the axes labels. Each panel shows a compilation of the manifolds for the systems defined by the ζ_i values and α . All panels have results for $a = \gamma - 2$, for reasons noted in the text (see the discussion of eq 4.1).

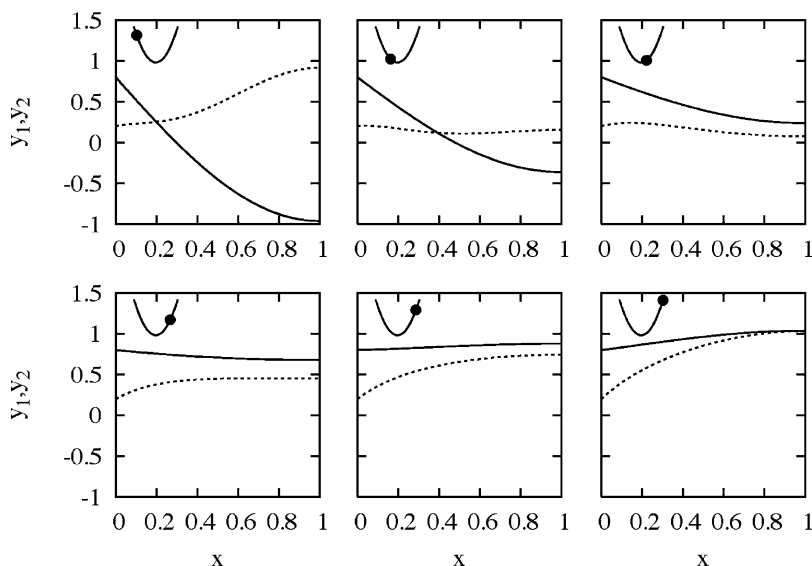


Figure 13. Plots demonstrating how distributions change along a one-dimensional manifold. The solid lines show the value of y_1 , and the dashed lines y_2 . The position on the manifold is indicated by the inset picture in each panel. This case is one of the $\zeta_1 = 0.1$ examples in Figure 12. The values of the parameters are $\gamma = 74.65$, $D_1 = 2.84$, and $D_2 = 4.73$.

bedded in an infinite-dimensional space. A more mathematical investigation of the manifolds is outside the scope of the present project.

The work described in this paper focuses on bound domains and one particular type of boundary condition. It also limits transport processes to diffusion only. Changing these conditions will affect the results in this paper to varying degrees. All of the results presented in this paper depend on a discrete, but infinite, spectrum, so it seems likely that a purely continuous spectrum for a system with infinite extent might eliminate the manifolds studied here, although they might persist locally in space. A change in boundary conditions will change the energy spectra and thus the exponential factors in many of the equations presented in this paper (for example, eq 2.5). This change would thus affect the degree of attraction but should not affect the overall picture presented in the paper. It seems likely that the results presented here would be not change with the addition of advection, as long as there is sufficient dissipation for the

system to equilibrate. Purely hyperbolic systems²⁷ with no diffusion almost certainly would not possess the types of manifolds discussed in this paper.

Acknowledgment. This work was supported by the Office of Basic Energy Sciences, Division of Chemical Sciences, Geosciences, and Biosciences, U. S. Department of Energy, under Contract No. W-31-109-ENG-38.

Appendix A: A Hierarchy of Manifolds for the Diffusion Equation

As the diffusion equation relaxes to equilibrium, it proceeds through a series of manifolds, the last few of which are described in section IIA. This cascade can be understood by starting from a manifold described by the set of all functions with finite extent in the spectral space described in eq 2.5

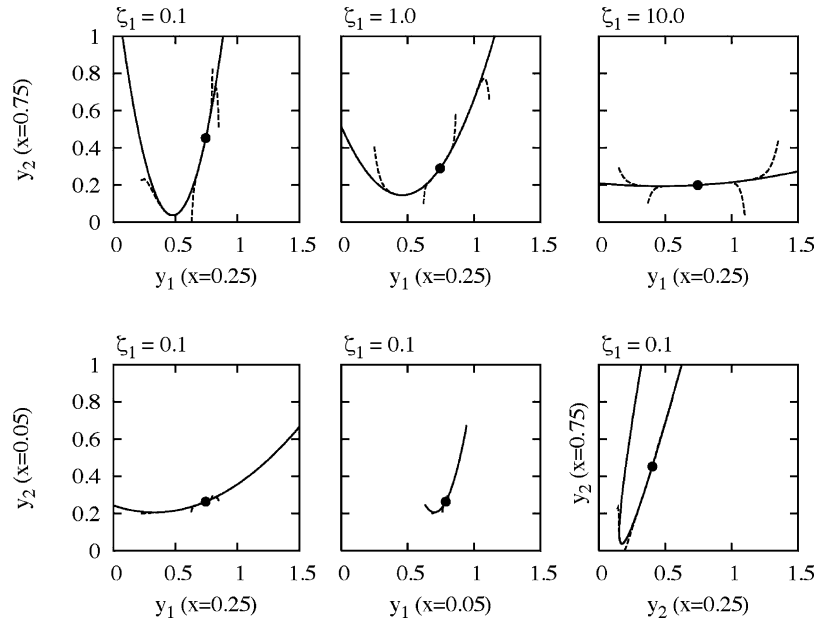


Figure 14. Panels showing how distributions are attracted to the one-dimensional manifolds. The manifolds are plotted as solid lines and are manifolds for a single system chosen from Figure 12. The dashed lines show the results for a set of distributions. The top left panel and the panels in the bottom row are all different projections of the same manifold and set of distributions.

$$y(x,t) = y_0 + \sum_{m=0}^{n-1} a_m e^{-(m+1/2)^2 \pi^2 D t} \sin\left(m + \frac{1}{2}\right) \pi x \quad (\text{A.1})$$

This equation defines an n -dimensional manifold in the infinite-dimensional system. To parametrize the manifold, consider the set of coordinates

$$u_0 = y(x_\beta) - y_0, u_1 = y(x_\sigma) - y_0, \dots \quad (\text{A.2})$$

that are described by the following matrix-vector product

$$\mathbf{u}^n = \mathbf{A}^n \mathbf{d}^n \quad (\text{A.3})$$

where the superscripts refer to the sizes of the vectors and the square matrix, which has the following matrix elements

$$(\mathbf{A}^n)_{km} = \sin\left(m + \frac{1}{2}\right) x_k \quad (\text{A.4})$$

and the x_k values refer to x_β , x_σ , etc. The vector \mathbf{d} is described as

$$d_m = a_m e^{-(m+1/2)^2 \pi^2 D t} \quad (\text{A.5})$$

One can observe that all matrix elements of \mathbf{A}^{n-1} are contained in \mathbf{A}^n , in the same order as they appear there, as well as for the vectors \mathbf{d} and \mathbf{u} . The elements of the vector \mathbf{d}^n are now calculated by matrix inversion

$$\mathbf{d}^n = (\mathbf{A}^n)^{-1} \mathbf{u}^n \quad (\text{A.6})$$

A point on the manifold is then described (see eq A.1)

$$u_n = \sum_{k=0}^{n-1} (a^{n+1})_{nk} d_k = \sum_{k=0}^{n-1} \sum_{m=0}^{n-1} (a^{n+1})_{nk} (a^n)_{km}^{-1} u_m \quad (\text{A.7a})$$

$$u_n = y(x_\phi) - y^{\text{eq}}(x_\phi) \quad (\text{A.7b})$$

with eq A.7b showing how a point on the manifold is evaluated

in the original species coordinates, with x_ϕ being the same as x_n in the matrix notation.

Equation A.7a is compared to the n -dimensional manifold for the system whose dimension is $n + 1$, which is described by the matrix \mathbf{A}^{n+1} . When the dimension in eq A.6 is increased, the n -dimensional manifold for the $(n + 1)$ -dimensional system is described by $(\mathbf{d})_n^{n+1} = 0$. The n -dimensional manifold is

$$(\mathbf{d}^{n+1})_n = 0 = \sum_{m=0}^n (a^{n+1})_{nm}^{-1} u_m \quad (\text{A.8a})$$

$$u_n = \frac{-1}{(a^{n+1})_{nn}^{-1}} \sum_{m=0}^{n-1} (a^{n+1})_{nm}^{-1} u_m \quad (\text{A.8b})$$

To establish that the system is relaxing through of series of manifolds, eqs A.7a and A.8a need to be compared term by term as a function of m . Starting with the m th term in eq A.8b and using the method of minors to find the inverse³⁹

$$\frac{-(a^{n+1})_{nm}^{-1}}{(a^{n+1})_{nn}^{-1}} = \frac{-A_{mn}}{\det(a^n)} \quad (\text{A.9})$$

where A_{mn} is the algebraic complement of \mathbf{A} . The algebraic complement can be written as the sum of a set of determinants

$$\frac{-A_{mn}}{\det(a^n)} = \frac{-1}{\det(a^n)} \sum_{k=0}^{n-1} (-1)^{n+m} (a^{n+1})_{nk} \det(a^n)_{km}^{-1} \quad (\text{A.10})$$

With some algebra and the definition of determinants, it can be shown

$$\frac{-1}{\det(a^n)} \sum_{k=0}^{n-1} (-1)^{n+m} (a^{n+1})_{nk} \det(a^n)_{km}^{-1} = \sum_{k=0}^{n-1} (a^{n+1})_{nk} (a^n)_{km}^{-1} \quad (\text{A.11})$$

which proves that eqs A.7a and A.8a are equal and that the system cascades through of series of surfaces defined by

truncated spectral decompositions. Because “ n ” in eqs A.7a and A.8 is arbitrary, this demonstrates that there is a cascade of manifolds of decreasing dimension as the system relaxes to equilibrium.

It is clear from the definition of the manifold derived from eq A.8a that the attraction is exponential in time. In general, the attractiveness of the manifold is more difficult to define in phase space but is straightforward in the coordinate u values. Here it is assumed that the approach to an n -dimensional manifold starts with the $(n + 1)$ -dimensional manifold, and with a little algebra the following form for the attraction is derived

$$\frac{u_n}{u_{n0}} = \left(\frac{u_{n+1}}{u_{n+10}} \right)^{[(n+1)+1/2]^2/(n+1/2)^2} \quad (\text{A.12})$$

which is a result described section IIA. The initial values, u_{n0} , are derived from d_{n0} in eq A.6.

Appendix B: Dynamical-Systems Analysis

Consider the system of nonlinear reaction–diffusion equations

$$\frac{\partial y_i}{\partial t} = F_i(y_1, \dots, y_i, \dots, y_n) + D_i \frac{\partial^2 y_i}{\partial x^2} \quad (\text{B.1})$$

The index “ i ” refers here and in subsequent equations to an individual species. The system of equations in eq B.1 is solved once again with a semidiscrete method³¹ as in section IIB.2. The system is written as a set of ordinary differential equations

$$\frac{\partial y_{ik}}{\partial t} = F(y_{1k}, \dots, y_{ik}, \dots, y_{nk}) + \frac{D}{\Delta x^2} (y_{i(k+1)} - 2y_{ik} + y_{i(k-1)}) \quad (\text{B.2})$$

The second index refers to a point on the grid. Once again it is assumed that the grid is evenly spaced. For n species on m grid points there are $r = n \times m$ coupled ordinary differential equations. To ensure accuracy, it is advisable to increase the number of grid points until convergence is reached.

The linearization and subsequent stability analysis in section IIB.2 can be extended to the system in eq B.2. For the i th species, linearization gives

$$\frac{\partial(\delta y)_i}{\partial t} = \sum_j J_{ij}(\delta y)_j \quad (\text{B.3})$$

\mathbf{J} describes localized linear dynamics for the function space. It is an infinite-dimensional matrix, which is evaluated here on a grid of points, to make it finite-dimensional. \mathbf{J} is defined in the following sub-block manner

$$\mathbf{J} = \begin{pmatrix} \mathbf{J}^{11} & \dots & \mathbf{J}^{1n} \\ \dots & \dots & \dots \\ \dots & \mathbf{J}^{ik} & \dots \\ \dots & \dots & \dots \\ \mathbf{J}^{n1} & \dots & \mathbf{J}^{nn} \end{pmatrix} \quad (\text{B.4})$$

The index “ k ” again refers to a grid point, and “ i ” labels the species. For n species defined on m grid points, each sub-block \mathbf{J}^{ik} has dimension $m \times m$, and the total dimension of \mathbf{J} is $r \times r$, where $r = nm$. When \mathbf{J} is defined in this manner it is made clear that an eigenvector of the finite-dimensional version of this matrix consists of n sections referring to the n species, and each section has a length m . It is understood that to study the eigenvalues and eigenvectors of \mathbf{J} it is necessary to numerically converge the eigenvectors of interest. From experience, the eigenvalues and eigenvectors with the lowest magnitude eigenvalues converge first. Because the eigenvalues are all negative in the calculations presented here, the first nonzero eigenvalue to converge is the “least negative”.

To make the discussion more concrete, consider the following system

$$\frac{\partial y_1}{\partial t} = -k_1 y_1 + k_2 y_2^2 + D_1 \frac{\partial^2 y_1}{\partial x^2} \quad (\text{B.5a})$$

$$\frac{\partial y_2}{\partial t} = 2k_1 y_1 - 2k_2 y_2^2 + D_2 \frac{\partial^2 y_2}{\partial x^2} \quad (\text{B.5b})$$

The semidiscrete method gives a grid of m points for each species and a system of ordinary differential equations

$$\frac{dy_{1k}}{dt} = -k_1 y_{1k} + k_2 (y_{2k})^2 + \frac{D_1}{(\Delta x)^2} [y_{1(k+1)} - 2y_{1k} + y_{1(k-1)}] \quad (\text{B.6a})$$

$$\frac{dy_{2k}}{dt} = 2k_1 y_{1k} - 2k_2 (y_{2k})^2 + \frac{D_2}{(\Delta x)^2} [y_{2(k+1)} - 2y_{2k} + y_{2(k-1)}] \quad (\text{B.6b})$$

where “ k ” refers to the k th grid point out of m and it is again assumed that the grid is evenly spaced. In eqs B.6a and B.6b the second derivative has been replaced by a finite-difference approximation. These equations are solved with an integrator for ordinary differential equations, with LSODE used here.⁴⁰ The boundary conditions are those in section IIB and these conditions once again define the points along the boundary as well as the finite-difference approximation for the second derivatives of the points adjacent to the boundary.

The Jacobian matrix for the system is written in the following form

$$\mathbf{J} = \begin{pmatrix} J^{11} & J^{12} \\ J^{21} & J^{22} \end{pmatrix} \quad (\text{B.7})$$

The matrix elements in the blocks for points away from the boundary are

$$J_{kk}^{11} = -k_1 - \frac{2D_1}{\Delta x^2} \quad J_{k,k+1}^{11} = J_{k,k-1}^{11} = \frac{D_1}{\Delta x^2} \\ J_{km}^{11} = 0 \text{ for all other } m \text{ values} \quad (\text{B.8a})$$

$$J_{kk}^{21} = 2k_1 \quad J_{km}^{21} = 0 \text{ for all other } m \text{ values} \quad (\text{B.8b})$$

$$J_{kk}^{12} = 2k_2 y_{2k} \quad J_{km}^{12} = 0 \text{ for all other } m \text{ values} \quad (\text{B.8c})$$

$$J_{kk}^{22} = -4k_2 y_{2k} - \frac{2D_2}{\Delta x^2} \quad J_{k,k+1}^{11} = J_{k,k-1}^{11} = \frac{D_2}{\Delta x^2}$$

$$J_{km}^{11} = 0 \text{ for all other } m \text{ values} \quad (\text{B.8d})$$

where the y values are equilibrium values. Points adjacent to the boundary have different matrix elements.

The converged eigenvectors of eq B.8 define low-dimensional, attractive manifolds near the equilibrium distribution, as they do for ordinary differential equations.²² The eigenvector of the least negative eigenvalue defines a one-dimensional manifold. The subspace of this eigenvector and the eigenvector whose eigenvalue is the next lowest defines a two-dimensional manifold, etc. Near equilibrium, they define a hierarchy of relaxation times.

Appendix C: Isomerization with Diffusion

Equations 3.4a and 3.4b define a series of 2×2 matrix-vector products

$$\begin{pmatrix} \frac{db_{1m}}{dt} \\ \frac{db_{2m}}{dt} \end{pmatrix} = \begin{pmatrix} -\left[k_1 + \left(m + \frac{1}{2}\right)^2 \pi^2 D_1\right] k_2 \\ k_1 \quad -\left[k_2 + \left(m + \frac{1}{2}\right)^2 \pi^2 D_2\right] \end{pmatrix} \begin{pmatrix} b_{1m} \\ b_{2m} \end{pmatrix} \quad (\text{C.1a})$$

$$\frac{\partial}{\partial t} \mathbf{b}^m = \mathbf{Z}^m \mathbf{b}^m \quad (\text{C.1b})$$

with \mathbf{Z}^m and \mathbf{b}^m in eq C.1b defined in eq C.1a. The matrix \mathbf{Z} is diagonalized in the same manner as \mathbf{J} in eq 2.30, and this leads to the following for the time development of the distributions

$$y_1(x,t) = y_1^{\text{eq}}(x) + \sum_{m=0} \{ [R_{11}^m (L_{11}^m b_{1m} + L_{21}^m b_{2m}) e^{\lambda_{1m} t} + R_{12}^m (L_{12}^m b_{1m} + L_{22}^m b_{2m}) e^{\lambda_{2m} t}] \} \sin\left(m + \frac{1}{2}\right) \pi x \quad (\text{C.2a})$$

$$y_2(x,t) = y_2^{\text{eq}}(x) + \sum_{m=0} \{ [R_{21}^m (L_{11}^m b_{1m} + L_{21}^m b_{2m}) e^{\lambda_{1m} t} + R_{22}^m (L_{12}^m b_{1m} + L_{22}^m b_{2m}) e^{\lambda_{2m} t}] \} \sin\left(m + \frac{1}{2}\right) \pi x \quad (\text{C.2b})$$

where \mathbf{R} and \mathbf{L} refer again to left and right eigenvectors, which are labeled by “ m ”. The eigenvalues λ_{1m} and λ_{2m} result from the diagonalization of \mathbf{Z}^m and are

$$\lambda_{1m} = \frac{1}{2} [\text{Tr}(\mathbf{Z}^m) + \Lambda^m] \quad (\text{C.3a})$$

$$\lambda_{2m} = \frac{1}{2} [\text{Tr}(\mathbf{Z}^m) - \Lambda^m] \quad (\text{C.3b})$$

$$\text{Tr}(\mathbf{Z}^m) = -(k_1 + k_2) - \left(m + \frac{1}{2}\right)^2 \pi^2 (D_1 + D_2) \quad (\text{C.3c})$$

$$\Lambda^m = \frac{1}{2} \sqrt{(k_1 + k_2)^2 + 2\left(m + \frac{1}{2}\right)^2 \pi^2 (k_1 - k_2)(D_1 - D_2) + \left(m + \frac{1}{2}\right)^4 \pi^4 (D_1 - D_2)^2} \quad (\text{C.4d})$$

Appendix D: A Hierarchy of Manifolds for Linear Reaction–Diffusion Systems

The relaxation of the two-species linear reaction–diffusion system of section IIIA (eqs 3.1a and 3.1b) is more complicated

than the diffusion equation of section IIA and Appendix A, and the analysis here is more limited than that in Appendix A. In analogy to eq A.1, sets of functions described by truncated expansions are studied. These functions are relaxed versions of the full time dependence of eqs C.2a and C.2b and are written as

$$y_1(x,t) = y_1^{\text{eq}}(x) + \left\{ \sum_{m=0}^{n-1} R_{11}^m (L_{11}^m b_{1m} + L_{21}^m b_{2m}) \sin\left[\left(m + \frac{1}{2}\right) \pi x\right] e^{\lambda_{1m} t} \right\} + R_{12}^0 (L_{12}^0 b_{10} + L_{22}^0 b_{20}) \sin\left(\frac{\pi x}{2}\right) e^{\lambda_{20} t} \quad (\text{D.1a})$$

$$y_2(x,t) = y_2^{\text{eq}}(x) + \left\{ \sum_{m=0}^{n-1} R_{21}^m (L_{11}^m b_{1m} + L_{21}^m b_{2m}) \sin\left[\left(m + \frac{1}{2}\right) \pi x\right] e^{\lambda_{1m} t} \right\} + R_{22}^0 (L_{12}^0 b_{10} + L_{22}^0 b_{20}) \sin\left(\frac{\pi x}{2}\right) e^{\lambda_{20} t} \quad (\text{D.1b})$$

Equations D.1a and D.1b define an $(n + 1)$ -dimensional manifold. The limit “ n ” is defined from the eigenvalue spectra denoted by the eigenvalues λ_{1m} and λ_{2m}

$$\lambda_{1(n-1)} > \lambda_{20} > \lambda_{1n} \quad (\text{D.2})$$

where it is assumed that in the physical situations studied (see section IIIB), all of the λ values are negative. For the situation outlined in eq D.2, the n -dimensional manifold is defined from the following truncation

$$y_1(x,t) = y_1^{\text{eq}}(x) + \sum_{m=0}^{n-1} R_{11}^m (L_{11}^m b_{1m} + L_{21}^m b_{2m}) \sin\left[\left(m + \frac{1}{2}\right) \pi x\right] e^{\lambda_{1m} t} \quad (\text{D.3a})$$

$$y_2(x,t) = y_2^{\text{eq}}(x) + \sum_{m=0}^{n-1} R_{21}^m (L_{11}^m b_{1m} + L_{21}^m b_{2m}) \sin\left[\left(m + \frac{1}{2}\right) \pi x\right] e^{\lambda_{1m} t} \quad (\text{D.3b})$$

The $(n + 1)$ -dimensional manifold of eqs D.1a and D.1b can be defined in many different coordinate systems in the space of species. Consider the following definitions

$$u_0 = y_1(x_\beta) - y_1^{\text{eq}}(x_\beta), \dots, u_{n+1} = y_1(x_\sigma) - y_1^{\text{eq}}(x_\sigma) \quad (\text{D.4a})$$

$$d_m = (L_{11}^m b_{1m} + L_{21}^m b_{2m}) e^{\lambda_{1m} t} \quad m \leq n - 1$$

$$d_n = (L_{12}^0 b_{10} + L_{22}^0 b_{20}) e^{\lambda_{20} t} \quad (\text{D.4b})$$

As in Appendix A, define a matrix \mathbf{A}

$$(\mathbf{A}^n)_{km} = R_{11}^m \sin\left(m + \frac{1}{2}\right) \pi x_k \quad m \leq n - 1 \quad (\text{D.5a})$$

$$(\mathbf{A}^n)_{kn} = R_{12}^0 \sin\left(\frac{\pi x_k}{2}\right) \quad (\text{D.5b})$$

The u values are described by the following matrix-vector product

$$\mathbf{u}^n = \mathbf{A}^n \mathbf{d}^n \quad (\text{D.6})$$

and the d values by

$$\mathbf{d}^n = (\mathbf{A}^n)^{-1} \mathbf{u}^n \quad (\text{D.7})$$

To calculate the value of y_1 and y_2 on the $(n+1)$ -dimensional manifold, the following must be evaluated

$$y_1(x_{n+1}) - y_1^{\text{eq}}(x_{n+1}) = u_{n+1} = \sum_{k=0}^n (a^{n+1})_{nk} d_k = \sum_{k=0}^n \sum_{m=0}^n (a^{n+1})_{nk} (a^n)_{km}^{-1} u_m \quad (\text{D.8a})$$

$$y_2(x_{n+1}) - y_2^{\text{eq}}(x_{n+1}) = \sum_{k=0}^n (b^{n+1})_{nk} d_k = \sum_{k=0}^n \sum_{m=0}^n (b^{n+1})_{nk} (a^n)_{km}^{-1} u_m \quad (\text{D.8b})$$

The elements of \mathbf{B} are

$$(\mathbf{B}^n)_{km} = R_{21}^m \sin\left(m + \frac{1}{2}\right) x_k \quad m \leq n-1 \quad (\text{D.9a})$$

$$(\mathbf{B}^n)_{kn} = R_{22}^0 \sin\left(\frac{\pi x_k}{2}\right) \quad (\text{D.9b})$$

The manifold can also be defined in a representation where the independent coordinates are y_2 values or in a mixture of y_1 values and y_2 values, and in different parts of the paper this is what is done.

The manifold defined in eqs D.8a and D.8b relaxes. The new manifold reached via this relaxation is defined by

$$(d^{n+1})_n = 0 = \sum_{m=0}^n (a^{n+1})_{nm}^{-1} u_m \quad (\text{D.10})$$

A similar analysis to what was done in Appendix A.1 demonstrates that eq D.10 defines a manifold that is the same as that generated from eqs D.3a and D.3b. The relaxation of the manifolds occurs, and the methodology of Appendix A can be applied

$$\frac{u_n}{u_{n0}} = \left(\frac{u_{n+1}}{u_{n+10}}\right)^{\lambda_{20}/\lambda_{1n}} \quad (\text{D.11a})$$

$$\frac{u_{n-1}}{u_{n-10}} = \left(\frac{u_n}{u_0}\right)^{\lambda_{1n}/\lambda_{1(n-1)}} \quad (\text{D.11b})$$

Appendix E: Nonlinear Reaction Diffusion System

Equations 4.2a and 4.2b can be solved exactly

$$y_1(x,t) = y_1^{\text{eq}} + \sum_{m=0} b_{1m} \sin\left[\left(m + \frac{1}{2}\right)\pi x\right] e^{-[1+(m+1/2)^2\pi^2 D_1]t} \quad (\text{E.1a})$$

$$y_2 = y_2^{\text{eq}} + \sum_m \sin\left[\left(m + \frac{1}{2}\right)\pi x\right] \left[b_{2m} - \sum_k \sum_n \frac{ab_{1k}b_{1n}r_{kn}^m}{(\gamma-2) + \left(m + \frac{1}{2}\right)^2\pi^2 D_2 - \left[\left(k + \frac{1}{2}\right)^2 + \left(n + \frac{1}{2}\right)^2\right]\pi^2 D_1} - \sum_j \frac{2b_{1j}as_j^m}{(\gamma-1) + \left(m + \frac{1}{2}\right)^2\pi^2 D_2 - \left(j + \frac{1}{2}\right)^2\pi^2 D_1} \right] e^{-[\gamma+(m+1/2)^2\pi^2 D_2]t} + \sum_m \sin\left[\left(m + \frac{1}{2}\right)\pi x\right] \times \left[\sum_k \sum_n \frac{ab_{1k}b_{1n}r_{kn}^m e^{-[2+((k+1/2)^2+(n+1/2)^2)\pi^2 D_1]t}}{(\gamma-2) + \left(m + \frac{1}{2}\right)^2\pi^2 D_2 - \left[\left(k + \frac{1}{2}\right)^2 + \left(n + \frac{1}{2}\right)^2\right]\pi^2 D_1} + \sum_j \frac{2b_{1j}as_j^m e^{-[1+(j+1/2)^2\pi^2 D_1]t}}{(\gamma-1) + \left(m + \frac{1}{2}\right)^2\pi^2 D_2 - \left(j + \frac{1}{2}\right)^2\pi^2 D_1} \right] \quad (\text{E.1b})$$

These equations relax asymptotically. To study one- and two-dimensional manifolds it is necessary to study the first two terms of the expansion in eq E.1a and the first two terms in the summations of eq E.1b. This gives the following asymptotic expressions for the two species

$$y_1(x,t) - y_1^{\text{eq}} = b_{10} \sin\left(\frac{\pi x}{2}\right) e^{-(1+\pi^2 D_1/4)t} + b_{11} \sin\left(\frac{3\pi x}{2}\right) e^{-(1+9\pi^2 D_1/4)t} \quad (\text{E.2})$$

The expansion for y_2 at long time consists of three different spatio-temporal factors

$$y_2(x,t) - y_2^{\text{eq}} = \tau_1(x,t) + \tau_2(x,t) + \tau_3(x,t) \quad (\text{E.3})$$

The terms τ_1 , τ_2 , and τ_3 are defined as

$$\tau_1(x,t) = e_{20} \sin\left(\frac{\pi x}{2}\right) e^{-(\gamma+\pi^2 D_2/4)t} + e_{21} \sin\left(\frac{3\pi x}{2}\right) e^{-(\gamma+9\pi^2 D_2/4)t} \quad (\text{E.4a})$$

$$\tau_2(x,t) = b_{10}^2 \tau_{20}(x) e^{-(2+\pi^2 D_1/2)t} + 2b_{10}b_{11} \tau_{21}(x) e^{-(2+5\pi^2 D_1/2)t} + b_{11}^2 \tau_{22}(x) e^{-(2+9\pi^2 D_1/2)t} \quad (\text{E.4b})$$

$$\tau_3(x,t) = b_{10} \tau_{30}(x) e^{-(1+\pi^2 D_1/4)t} + b_{11} \tau_{31}(x) e^{-(1+9\pi^2 D_1/4)t} \quad (\text{E.4c})$$

The quantities necessary to define τ_1 are

$$e_{20} = b_{20} - \sum_k \sum_n \frac{ab_{1k}b_{1n}r_{kn}^0}{(\gamma-2) + \frac{\pi^2 D_2}{4} - \left[\left(k + \frac{1}{2}\right)^2 + \left(n + \frac{1}{2}\right)^2\right]\pi^2 D_1} - \sum_j \frac{2b_{1j}as_j^0}{(\gamma-1) + \frac{\pi^2 D_2}{4} - \left(j + \frac{1}{2}\right)^2\pi^2 D_1} \quad (\text{E.5a})$$

$$e_{21} = b_{21} -$$

$$\sum_k \sum_n \frac{ab_{1k}b_{1n}r_{kn}^1}{(\gamma - 2) + \frac{9\pi^2 D_2}{4} - \left[\left(k + \frac{1}{2} \right)^2 + \left(n + \frac{1}{2} \right)^2 \right] \pi^2 D_1} - \sum_j \frac{2b_{1j}as_j^1}{(\gamma - 1) + \frac{9\pi^2 D_2}{4} - \left(j + \frac{1}{2} \right)^2 \pi^2 D_1} \quad (\text{E.5b})$$

The functions necessary to define τ_2 are

$$\tau_{20}(x) = \sum_m \frac{ar_{00}^m \sin \left[\left(m + \frac{1}{2} \right) \pi x \right]}{(\gamma - 2) + \left(m + \frac{1}{2} \right)^2 \pi^2 D_2 - \frac{\pi^2 D_1}{2}} \quad (\text{E.6a})$$

$$\tau_{21}(x) = \sum_m \frac{ar_{01}^m \sin \left[\left(m + \frac{1}{2} \right) \pi x \right]}{(\gamma - 2) + \left(m + \frac{1}{2} \right)^2 \pi^2 D_2 - \frac{5\pi^2 D_1}{2}} \quad (\text{E.6b})$$

$$\tau_{22}(x) = \sum_m \frac{ar_{11}^m \sin \left[\left(m + \frac{1}{2} \right) \pi x \right]}{(\gamma - 2) + \left(m + \frac{1}{2} \right)^2 \pi^2 D_2 - \frac{9\pi^2 D_1}{2}} \quad (\text{E.6c})$$

to define τ_3 are

$$\tau_{30}(x) = \sum_m \frac{2as_0^m \sin \left[\left(m + \frac{1}{2} \right) \pi x \right]}{(\gamma - 1) + \left(m + \frac{1}{2} \right)^2 \pi^2 D_2 - \frac{\pi^2 D_1}{4}} \quad (\text{E.7a})$$

$$\tau_{31}(x) = \sum_m \frac{2as_1^m \sin \left[\left(m + \frac{1}{2} \right) \pi x \right]}{(\gamma - 1) + \left(m + \frac{1}{2} \right)^2 \pi^2 D_2 - \frac{9\pi^2 D_1}{4}} \quad (\text{E.7b})$$

The terms in eqs E.3–E.7 are combined to define the one-dimensional and two-dimensional manifolds in section IV. The coefficients for the quadratic equation in eq G.13c are

$$\mu_1 = \tau_{20}(x_\sigma) \sin^2 \left(\frac{3\pi x_\beta}{2} \right) - 2\tau_{21}(x_\sigma) \sin \left(\frac{\pi x_\beta}{2} \right) \sin \left(\frac{3\pi x_\beta}{2} \right) + \tau_{22}(x_\sigma) \sin^2 \left(\frac{\pi x_\beta}{2} \right) \quad (\text{E.8a})$$

$$\mu_2 = 2\tau_{21}(x_\sigma)y_{1\beta} \sin \left(\frac{3\pi x_\beta}{2} \right) + \tau_{30}(x_\sigma) \sin^2 \left(\frac{3\pi x_\beta}{2} \right) - \tau_{31}(x_\sigma) \sin \left(\frac{\pi x_\beta}{2} \right) \sin \left(\frac{3\pi x_\beta}{2} \right) - 2\tau_{22}(x_\sigma)y_{1\beta} \sin \left(\frac{\pi x_\beta}{2} \right) \quad (\text{E.8b})$$

$$\mu_3 = \tau_{31}(x_\sigma)y_{1\beta} \sin \left(\frac{3\pi x_\beta}{2} \right) + \tau_{22}(x_\sigma)y_{1\beta}^2 - y_{2\sigma} \sin \left(\frac{3\pi x_\beta}{2} \right) \quad (\text{E.8c})$$

Appendix F: Attraction to One-Dimensional Manifolds for the Nonlinear Reaction–Diffusion System

In what follows, the coordinates describe a path starting with the projection enumerated in eqs G.13–G.15. The coordinates and α values are:

Case 1_1

$$\frac{u_1}{u_1^0} = \frac{2\mu_1 y_{1\beta} + [\mu_2 \mp \sqrt{\mu_2^2 - 4\mu_1 \mu_3}] \sin \left(\frac{\pi x}{2} \right)}{2\mu_1^0 y_{1\beta} + [\mu_2^0 \mp \sqrt{(\mu_2^0)^2 - 4\mu_1^0 \mu_3^0}] \sin \left(\frac{\pi x}{2} \right)} \quad (\text{F.1a})$$

$$\frac{u_2}{u_2^0} = \frac{-\mu_2 \pm \sqrt{\mu_2^2 - 4\mu_1 \mu_3}}{-\mu_2^0 \pm \sqrt{(\mu_2^0)^2 - 4\mu_1^0 \mu_3^0}} \quad (\text{F.1b})$$

$$\alpha_{11} = \frac{4 + 9\pi^2 D_1}{4 + \pi^2 D_1} \quad (\text{F.1c})$$

with the μ values defined in eq E.8 and terms such as μ_2^0 being obvious generalizations. They are formed by replacing terms such as $y_{1\beta}$ with $y_{1\beta}^0$. It is also straightforward, though tedious, to demonstrate the expected result that $u_1/u_1^0 = 0$ places the system on the one-dimensional manifold defined in eq 4.7. For the other cases, attraction takes the following forms:

Case 1_2

$$\frac{u_1}{u_1^0} = \frac{y_{2\sigma} \sin^2 \left(\frac{\pi x_\beta}{2} \right) - (y_{1\beta})^2 \tau_{20}(x_\sigma) - y_{1\beta} \tau_{30}(x_\sigma) \sin \left(\frac{\pi x_\beta}{2} \right)}{y_{2\sigma} \sin^2 \left(\frac{\pi x_\beta}{2} \right) - (y_{1\beta}^0)^2 \tau_{20}(x_\sigma) - (y_{1\beta}^0) \tau_{30}(x_\sigma) \sin \left(\frac{\pi x_\beta}{2} \right)} \quad (\text{F.2a})$$

$$\frac{u_2}{u_2^0} = \frac{y_{1\beta}}{y_{1\beta}^0} \quad (\text{F.2b})$$

$$\alpha_{12} = \frac{4\gamma + \pi^2 D_2}{4 + \pi^2 D_1} \quad (\text{F.2c})$$

Case 2_1

$$\frac{u_1}{u_1^0} = \frac{y_{2\sigma} \sin \left(\frac{\pi x_\beta}{2} \right) - y_{1\beta} \sin \left(\frac{\pi x_\sigma}{2} \right)}{y_{2\sigma}^0 \sin \left(\frac{\pi x_\beta}{2} \right) - y_{1\beta}^0 \sin \left(\frac{\pi x_\sigma}{2} \right)} \quad (\text{F.3a})$$

$$\frac{u_2}{u_2^0} = \frac{y_{2\sigma} \sin \left(\frac{3\pi x_\beta}{2} \right) - y_{1\beta} \sin \left(\frac{3\pi x_\sigma}{2} \right)}{y_{2\sigma}^0 \sin \left(\frac{3\pi x_\beta}{2} \right) - y_{1\beta}^0 \sin \left(\frac{3\pi x_\sigma}{2} \right)} \quad (\text{F.3b})$$

$$\alpha_{21} = \frac{4\gamma + 9\pi^2 D_2}{4\gamma + \pi^2 D_2} \quad (\text{F.3c})$$

Case 2_2

$$\frac{u_1}{u_1^0} = \frac{y_{1\beta}}{y_{1\beta}^0} \quad (\text{F.4a})$$

$$\frac{u_2}{u_2^0} = \frac{y_{2\sigma} \sin^2\left(\frac{\pi x_\beta}{2}\right) - (y_{1\beta})^2 \tau_{20}(x_\sigma) - y_{1\beta} \tau_{30}(x_\sigma) \sin\left(\frac{\pi x_\beta}{2}\right)}{y_{2\sigma} \sin^2\left(\frac{\pi x_\beta}{2}\right) - (y_{1\beta}^0)^2 \tau_{20}(x_\sigma) - (y_{1\beta}^0) \tau_{30}(x_\sigma) \sin\left(\frac{\pi x_\beta}{2}\right)} \quad (\text{F.4b})$$

$$\alpha_{22} = \frac{4 + \pi^2 D_1}{4\gamma + \pi^2 D_2} \quad (\text{F.4c})$$

Appendix G: Two-Dimensional Manifolds

This appendix summarizes information for the two-dimensional manifolds studied in section IIB.1, section III, and section IV.

1. Irreversible Unimolecular Reaction. For the system in section IIB.2 it is possible to define higher-dimensional manifolds, because of the ordering of the eigenvalues. A two-dimensional manifold is a plane and is written as

$$y_\phi = \frac{1}{\chi(x_\sigma, x_\beta)} [\chi(x_\sigma, x_\phi) y_\beta + \chi(x_\beta, x_\phi) y_\sigma] \quad (\text{G.1a})$$

$$\chi(z_1, z_2) = \sin\left(\frac{\pi z_1}{2}\right) \sin\left(\frac{3\pi z_2}{2}\right) - \sin\left(\frac{\pi z_2}{2}\right) \sin\left(\frac{3\pi z_1}{2}\right) \quad (\text{G.1b})$$

where the notation of eq 2.19 has been extended in an obvious way to a third point at x_ϕ .

2. Isomerization with Diffusion. There are two types of two-dimensional manifolds for this system depending on the ordering of the eigenvalues. The first two eigenvalues are either

$$\text{case 1 } \lambda_{10} > \lambda_{11} \quad (\text{G.2a})$$

or

$$\text{case 2 } \lambda_{10} > \lambda_{20} \quad (\text{G.2b})$$

with the designation of the eigenvalues described in Appendix C. Because all eigenvalues are negative, these are the largest two, or “least negative”. The calculation of the manifolds follows from section II. There are a number of ways to project the two-dimensional manifolds for a system of two species. The independent coordinates used here will be $y_{1\beta}$ and $y_{2\sigma}$. For case 1, with this projection, the two-dimensional manifold defines a point along y_1 as

$$y_{1\phi} = g_{11} y_{1\beta} + g_{12} y_{2\sigma} \quad (\text{G.3a})$$

$$g_{11} = \frac{1}{q} \left[R_{11}^0 R_{21}^1 \sin\left(\frac{3\pi x_\sigma}{2}\right) \sin\left(\frac{\pi x_\phi}{2}\right) - R_{11}^1 R_{21}^0 \sin\left(\frac{\pi x_\sigma}{2}\right) \sin\left(\frac{3\pi x_\phi}{2}\right) \right] \quad (\text{G.3b})$$

$$g_{12} = \frac{R_{11}^0 R_{11}^1}{q} \left[\sin\left(\frac{\pi x_\beta}{2}\right) \sin\left(\frac{3\pi x_\phi}{2}\right) - \sin\left(\frac{3\pi x_\beta}{2}\right) \sin\left(\frac{\pi x_\phi}{2}\right) \right] \quad (\text{G.3c})$$

$$q = R_{21}^1 R_{11}^0 \sin\left(\frac{\pi x_\beta}{2}\right) \sin\left(\frac{3\pi x_\sigma}{2}\right) - R_{21}^0 R_{11}^1 \sin\left(\frac{\pi x_\sigma}{2}\right) \sin\left(\frac{3\pi x_\beta}{2}\right) \quad (\text{G.3d})$$

It defines a point along the distribution of y_2 as

$$y_{2\phi} = g_{21} y_{1\beta} + g_{22} y_{2\sigma} \quad (\text{G.4a})$$

$$g_{21} = \frac{R_{21}^0 R_{21}^1}{q} \left[\sin\left(\frac{3\pi x_\sigma}{2}\right) \sin\left(\frac{\pi x_\phi}{2}\right) - \sin\left(\frac{\pi x_\sigma}{2}\right) \sin\left(\frac{3\pi x_\phi}{2}\right) \right] \quad (\text{G.4b})$$

$$g_{22} = \frac{1}{q} \left[R_{21}^1 R_{11}^0 \sin\left(\frac{\pi x_\beta}{2}\right) \sin\left(\frac{3\pi x_\phi}{2}\right) - R_{21}^0 R_{11}^1 \sin\left(\frac{3\pi x_\beta}{2}\right) \sin\left(\frac{\pi x_\phi}{2}\right) \right] \quad (\text{G.4c})$$

where the notation of eqs 3.8a and 3.8b is used and extended. Because of the linearity of the system, the two-dimensional manifolds are planes.

Through the use of the same projection as in eqs G.3 and G.4, a two-dimensional manifold for case 2 defines a point along the y_1 -distribution as

$$y_{1\phi} = \frac{\sin\left(\frac{\pi x_\phi}{2}\right)}{\sin\left(\frac{\pi x_\beta}{2}\right)} y_{1\beta} \quad (\text{G.5})$$

It defines a point along the y_2 -distributions as

$$y_{2\phi} = \frac{\sin\left(\frac{\pi x_\phi}{2}\right)}{\sin\left(\frac{\pi x_\sigma}{2}\right)} y_{2\sigma} \quad (\text{G.6})$$

To describe the attraction to a two-dimensional manifold a further description of the eigenvalue spectrum is necessary. First, expand the list of cases in the following manner

$$\text{case 1}_1 \quad \lambda_{10} > \lambda_{11} > \lambda_{12} \quad (\text{G.7a})$$

$$\text{case 1}_2 \quad \lambda_{10} > \lambda_{11} > \lambda_{20} \quad (\text{G.7b})$$

and

$$\text{case 2}_1 \quad \lambda_{10} > \lambda_{20} > \lambda_{11} \quad (\text{G.7c})$$

Only one case is described here. Through the use of the formalism outlined here and in Appendix D, all projections of all cases are straightforward. There are three coordinates that describe the approach to a two-dimensional manifold and the subsequent motion on it, if it is assumed that the system passes through a three-dimensional manifold as it relaxes to the two-dimensional manifold. The behaviors of these coordinates in phase space are once again straightforward

$$\frac{u_2}{u_2^0} = \left(\frac{u_3}{u_3^0}\right)^{\alpha_{11}} \quad (\text{G.8a})$$

$$\frac{u_1}{u_1^0} = \left(\frac{u_2}{u_2^0}\right)^{\alpha_{12}} \quad (\text{G.8b})$$

where the α values are

$$\alpha_{11} = \frac{\lambda_{11}}{\lambda_{10}} \quad (\text{G.9a})$$

$$\alpha_{12} = \frac{\lambda_{12}}{\lambda_{11}} \quad (\text{G.9b})$$

The u -coordinates can be written in the manner of Appendix D. The u_1 -coordinate is

$$\frac{u_1}{u_1^0} = \frac{c_{31}y_{1\beta} + c_{32}y_{2\sigma} + c_{33}y_{2\phi}}{c_{31}y_{1\beta}^0 + c_{32}y_{2\sigma}^0 + c_{33}y_{2\phi}^0} \quad (\text{G.10})$$

The matrix elements are

$$c_{31} = R_{21}^0 R_{21}^1 \left[\sin\left(\frac{\pi x_\sigma}{2}\right) \sin\left(\frac{3\pi x_\phi}{2}\right) - \sin\left(\frac{3\pi x_\sigma}{2}\right) \sin\left(\frac{\pi x_\phi}{2}\right) \right] \quad (\text{G.11a})$$

$$c_{32} = R_{11}^1 R_{21}^0 \sin\left(\frac{\pi x_\phi}{2}\right) \sin\left(\frac{3\pi x_\beta}{2}\right) - R_{11}^0 R_{21}^1 \sin\left(\frac{\pi x_\beta}{2}\right) \sin\left(\frac{3\pi x_\phi}{2}\right) \quad (\text{G.11b})$$

$$c_{33} = R_{11}^0 R_{21}^1 \sin\left(\frac{\pi x_\beta}{2}\right) \sin\left(\frac{3\pi x_\sigma}{2}\right) - R_{11}^1 R_{21}^0 \sin\left(\frac{3\pi x_\beta}{2}\right) \sin\left(\frac{\pi x_\sigma}{2}\right) \quad (\text{G.11c})$$

Equations G.11a–G.11c demonstrate that as the system relaxes and $u_1 \rightarrow 0$, it relaxes to the two-dimensional manifold shown in eqs G.3a–G.3c, as expected from Appendix D.

In terms of the variables ζ_1 , ζ_2 , and ζ_3 , the attractiveness of the two-dimensional manifolds has three possible values

$$\alpha_{11} = \frac{\lambda_{12}}{\lambda_{11}} = \frac{4 + 25\pi^2\zeta_1 - \sqrt{16 + 200\pi^2\zeta_2\zeta_3 + 625\pi^4\zeta_2^2}}{4 + 9\pi^2\zeta_1 - \sqrt{16 + 72\pi^2\zeta_2\zeta_3 + 81\pi^4\zeta_2^2}} \quad (\text{G.12a})$$

$$\alpha_{12} = \frac{\lambda_{20}}{\lambda_{11}} = \frac{4 + \pi^2\zeta_1 + \sqrt{16 + 8\pi^2\zeta_2\zeta_3 + \pi^4\zeta_2^2}}{4 + 9\pi^2\zeta_1 - \sqrt{16 + 72\pi^2\zeta_2\zeta_3 + 81\pi^4\zeta_2^2}} \quad (\text{G.12b})$$

$$\alpha_{21} = \frac{\lambda_{11}}{\lambda_{20}} = \frac{1}{\alpha_{22}} \quad (\text{G.12c})$$

3. Nonlinear Reaction–Diffusion System. There are numerous ways to represent the two-dimensional manifolds for the four cases in eq 4.6. Only one set of independent variables is shown for each case. It is not difficult to derive other projections. Once again, points on both distributions can be defined in terms

of the two-dimensional manifolds. The bases for the representations of the manifolds are in eqs E.3–E.7 of Appendix E. Without derivation, the representations are enumerated:

Case 1_1

$$y_{1\phi} = \chi_{11}(x_\beta, x_\sigma) \sin\left(\frac{\pi x_\phi}{2}\right) + \xi_{11}(x_\beta, x_\sigma) \sin\left(\frac{3\pi x_\phi}{2}\right) \quad (\text{G.13a})$$

$$y_{2\phi} = \tau_{30}(x_\phi)\chi_{11}(x_\beta, x_\sigma) + \tau_{31}(x_\phi)\xi_{11}(x_\beta, x_\sigma) +$$

$$\tau_{20}(x_\phi)\chi_{11}^2(x_\beta, x_\sigma) + 2\tau_{21}(x_\phi)\chi_{11}(x_\beta, x_\sigma)\xi_{11}(x_\beta, x_\sigma) \quad (\text{G.13b})$$

$$\chi_{11} = \frac{-\mu_2 \pm \sqrt{\mu_2^2 - 4\mu_1\mu_3}}{2\mu_1} \quad (\text{G.13c})$$

$$\xi_{11} = \frac{y_{1\beta} - \chi_{11} \sin\left(\frac{\pi x_\beta}{2}\right)}{\sin\left(\frac{3\pi x_\beta}{2}\right)} \quad (\text{G.13d})$$

The forms of μ_1 , μ_2 , and μ_3 are presented in Appendix E, eq E.8. Another case is:

Case 2_1

$$y_1(x) = y_1^{\text{eq}}(x) \quad (\text{G.14a})$$

$$y_{2\phi} = \frac{1}{\chi(x_\sigma, x_\beta)} [\chi(x_\sigma, x_\phi)y_{2\beta} + \chi(x_\beta, x_\phi)y_{2\sigma}] \quad (\text{G.14b})$$

This representation is merely the same as the one in section II, with the same notation for the transformation function χ from eq 2.1. The final two cases are:

Cases 1_2 and 2_2

$$y_{1\phi} = \frac{\sin\left(\frac{\pi x_\phi}{2}\right)}{\sin\left(\frac{\pi x_\beta}{2}\right)} y_{1\beta} \quad (\text{G.15a})$$

$$y_{2\phi} = \chi_{12}(x_\beta, x_\sigma) \sin\left(\frac{\pi x_\phi}{2}\right) + \frac{y_{1\beta}^2 \tau_{20}(x_\phi)}{\sin^2\left(\frac{\pi x_\beta}{2}\right)} + \frac{y_{1\beta} \tau_{30}(x_\phi)}{\sin\left(\frac{\pi x_\beta}{2}\right)} \quad (\text{G.15b})$$

$$\chi_{12}(x_\beta, x_\sigma) = \frac{1}{\sin\left(\frac{\pi x_\sigma}{2}\right)} \left[y_{2\sigma} - \frac{\tau_{20}(x_\sigma) y_{1\beta}^2}{\sin^2\left(\frac{\pi x_\beta}{2}\right)} - \frac{\tau_{30}(x_\sigma) y_{1\beta}}{\sin\left(\frac{\pi x_\beta}{2}\right)} \right] \quad (\text{G.15c})$$

References and Notes

- (1) For example, see: (a) Oran E. S.; Boris, J. P. *Numerical Simulation of Reactive Flows*; Cambridge University Press: Cambridge, U. K., 2001. (b) Warnatz, J.; Maas, U.; Dibble, R. W. *Combustion*; Springer: New York, 2001. (c) Kee, R. J.; Coltrin, M. E.; Glarborg, P. *Chemical Reacting Flow: Theory and Practice*; Wiley-Interscience: New York, 2003.
- (2) (a) Griffiths, J. F. *Prog. Energy Combust. Sci.* **1995**, *21*, 25. (b) Tomlin, A. S.; Turányi, T.; Pilling, M. J. In *Low-Temperature Combustion and Autoignition*; Pilling, M. J., Ed.; Comprehensive Chemical Kinetics 35; Elsevier: New York, 1997; p 293. (c) Okino M. S.; Mavrouniotis, M. L. *Chem. Rev.* **1998**, *98*, 243.
- (3) Turányi, T.; Tomlin, A. S.; Pilling, M. J. *J. Phys. Chem.* **1993**, *97*, 163.

- (4) For example, see: (a) Nayfeh, A. H. *Introduction to Perturbation Techniques*; John Wiley & Sons: New York, 1981. (b) O'Malley, R. E. *Singular Perturbation Methods for Ordinary Differential Equations*; Applied Mathematical Sciences 89; Springer-Verlag: New York, 1991. (c) Holmes, M. H. *Introduction to Perturbation Methods*; Texts in Applied Mathematics 20; Springer-Verlag: New York, 1995. (d) Gorban, A. N.; Karlin I. *Phys. Rep.* **2004**, 369, 197.
- (5) Kaper, H. J.; Kaper, T. J. *Physica D* **2002**, 165, 66.
- (6) Roussel, M. R. A Rigorous Approach to Steady-State Kinetics Applied to Simple Enzyme Mechanisms. Ph.D. Thesis, University of Toronto, 1994.
- (7) Fraser, S. J. *J. Chem. Phys.* **1988**, 88, 4732.
- (8) (a) Roussel M. R.; Fraser, S. J. *J. Chem. Phys.* **1990**, 93, 1072. (b) Roussel M. R.; Fraser, S. J. *J. Chem. Phys.* **1991**, 94, 7106. (c) Roussel M. R.; Fraser, S. J. *J. Phys. Chem.* **1991**, 95, 8762. (d) Roussel, M. R.; Fraser, S. J. *J. Phys. Chem.* **1993**, 97, 8316. (e) Roussel, M. R.; Fraser, S. J. *J. Phys. Chem.* **1994**, 98, 5174. (f) Fraser S. J.; Roussel, M. R. *Can. J. Chem.* **1994**, 72, 800. (g) Fraser, S. J. *J. Chem. Phys.* **1998**, 109, 411.
- (9) (a) Nguyen, A. H.; Fraser, S. J. *J. Chem. Phys.* **1989**, 91, 186. (b) Roussel, M. R. *J. Math. Chem.* **1997**, 21, 385. (c) Roussel, M. R.; Fraser, S. J. *Chaos* **2001**, 11, 196.
- (10) Lam S. H.; Goussis, D. A. *Int. J. Chem. Kinet.* **1994**, 26, 461. For recent developments and important applications, for example, see: Valorani, M.; Najm, H. N.; Goussis, D. A. *Combust. Flame* **2003**, 134, 35 and references therein.
- (11) (a) Maas, U.; Pope, S. B. *Combust. Flame* **1992**, 88, 239. (b) Maas, U.; Pope, S. B. *Proc. Combust. Inst.* **1992**, 28, 103.
- (12) Maas, U.; Pope, S. B. *Proc. Combust. Inst.* **1994**, 25, 1349.
- (13) Recent applications and algorithm developments concerning the Maas-Pope algorithm by Maas and co-workers can be found in: (a) Maas, U. *Appl. Math.* **1995**, 3, 249. (b) Schmidt, D.; Maas, U.; Segatz, J.; Reidel, U.; Warnatz, J. *Combust. Sci. Technol.* **1996**, 113, 3. (c) Deuffhard, P.; Heroth, J.; Maas, U. In *Modeling of Chemical Reaction Systems, Proceedings of an International Workshop (Heidelberg)*; Warnatz J.; Behrendt, F., Eds.; Springer: Berlin, 1996. (d) Neimann, H.; Schmidt, D.; Maas, U. *J. Eng. Math.* **1997**, 31, 131. (e) Schmidt, D.; Blasenber, T.; Maas, U. *Combust. Theory Model.* **1998**, 2, 135. (f) Maas, U. *Comput. Visualization Sci.* **1998**, 1, 69. (g) Yan, X.; Maas, U. *Proc. Combust. Inst.* **2000**, 28, 1615.
- (14) Other recent applications and algorithm developments of the Maas-Pope algorithm can be found, for example, in: (a) Eggels, R. L. G. M.; de Goey, L. P. H. *Combust. Flame* **1995**, 100, 559. (b) Eggels, R. L. G. M.; de Goey, L. P. H. *Combust. Sci. Technol.* **1995**, 107, 165. (c) Deuffhard P.; Heroth, J. In *Scientific Computing in Chemical Engineering*; Keil, F., Mackens, W., Voss, H., Werther, J., Eds.; Springer: Berlin, 1996; p 29. (d) Eggels, R. L. G. M.; Louis, J. J. B.; Kok, B. W.; de Goey, L. P. H. *Combust. Sci. Technol.* **1997**, 123, 347. (e) Gicquel, O.; Thevenin, D.; Hilka M.; Darabiha, N. *Combust. Theory Model.* **1999**, 3, 479. (f) Rhodes, C.; Morari, M.; Wiggins, S. *Chaos* **1999**, 9, 108. (g) Singh, S.; Rastigejev, Y.; Paolucci, S.; Powers, J. M. *Combust. Theory Model.* **2001**, 5, 163.
- (15) Davis, M. J.; Skodje, R. T. *J. Chem. Phys.* **1999**, 111, 859.
- (16) Skodje, R. T.; Davis, M. J. *J. Phys. Chem. A* **2001**, 105, 10356.
- (17) Davis, M. J.; Skodje, R. T. *J. Phys. Chem.* **2001**, 215, 233.
- (18) Singh, S.; Powers, J. M.; Paolucci, S. *J. Chem. Phys.* **2002**, 117, 1482.
- (19) Lowe, R.; Tomlin, A. *Atmos. Environ.* **2000**, 34, 2425.
- (20) Schwer, Schwer; Lu, P.; Green, W. H.; Semiao, V. *Combust. Theory Model.* **2003**, 7, 383.
- (21) Lebiez, D. *J. Chem. Phys.* **2004**, 120, 6890.
- (22) Perko, L. *Differential Equations and Dynamical Systems*; Springer-Verlag: New York, 1996.
- (23) Yannacopoulos, A. N.; Tomlin, A. S.; Brindley, J.; Merkin, J. H.; Pilling, M. J. *Physica D* **1994**, 83, 421.
- (24) Hadjinicolaou M.; Goussis, D. A. *SIAM J. Sci. Comput.* **1999**, 20, 781.
- (25) Davis M. J. *J. Phys. Chem A* **2006**, 110, 5257.
- (26) Davis, M. J.; Zagaris, A. S.; Kaper, T. J. The effects of diffusion on chemical-kinetic reduction, manuscript to be submitted.
- (27) Logan, J. D. *Applied Partial Differential Equations*, 2nd ed.; Springer: New York, 2004.
- (28) For example, see: Kee, R. J.; Grcar, J. F.; Smooke, M. D.; Miller, J. A. A Fortran Program for Modeling Steady Laminar One-Dimensional Premixed Flames; SAND85-8240; Sandia National Laboratories: Albuquerque, NM, 1985.
- (29) Robinson, J. C. *Chaos* **1995**, 5, 330.
- (30) (a) Temam R. *Infinite-Dimensional Dynamical Systems in Mechanics and Physics*; Applied Mathematical Sciences 68; Springer-Verlag: New York, 1988. (b) Robinson, J. C. *Infinite-Dimensional Dynamical Systems: An Introduction to Dissipative Parabolic PDEs and the Theory of Global Attractors*; Cambridge University Press: Cambridge, U. K., 2001.
- (31) Hundsdorfer W.; Verwer, J. G. *Numerical Solution of Time-Dependent Advection-Diffusion-Reaction Equations*; Springer: Berlin, 2003.
- (32) Blom, J. G.; Zegeling, P. A. *ACM Trans. Software* **1994**, 20, 194.
- (33) *Handbook of Mathematical Functions*; Abramowitz, M., Stegun, I. A., Eds.; Dover: New York, 1965.
- (34) Local linearity stability analysis for ordinary differential equations is discussed in many places. For example, see ref 22.
- (35) Chapter 5.3 of ref 27 has a discussion of the stability analysis of partial differential equations.
- (36) Discussions of local linear stability analysis are less common for partial differential equations, but the generation and use of the linearization is an important part of numerical methods centered on semidiscrete methods. See, for example, ref 31 or Iserles, A. *A First Course in the Numerical Analysis of Differential Equations*; Cambridge University Press: Cambridge, U. K., 1996.
- (37) For example, see: Golub G. H.; Van Loan, C. F. *Matrix Computations*; Johns Hopkins University Press: Baltimore, MD, 1996.
- (38) Fabes, E.; Luskin, M.; Sell, G. R. *J. Diff. Eq.* **1991**, 89, 355.
- (39) Barnett, S. *Matrices: Methods and Applications*; Clarendon Press: Oxford, U. K., 1990.
- (40) Hindmarsh, A. C. In *Scientific Computing*; Stepleman, R. S. et al., Eds.; North-Holland: Amsterdam, 1983; p 55.